STRUCTURAL, MAGNETIC AND SURFACE PROPERTIES OF RF MAGNETRON SPUTTERED UNDOPED LANTHANUM MANGANITE THIN FILMS

by

VARAD RAJAN SAKHALKAR

Presented to the Faculty of the Graduate School of
The University of Texas at Arlington in Partial Fulfillment
of the Requirements
for the Degree of

MASTER OF SCIENCE IN MATERIALS SCIENCE AND ENGINEERING

THE UNIVERSITY OF TEXAS AT ARLINGTON

DECEMBER 2009

ACKNOWLEDGEMENTS

I am deeply thankful to Dr. Efstathios Meletis, my research advisor for offering a chance to work on this research project and his excellent guidance and help throughout the project. I am also thankful to Dr. Jin and Dr. Liu for accepting my request to participate as committee members for my thesis defense.

I am also grateful to Dr. Jiechao Jiang and Mr. Yinsheng Fang for helping me in TEM characterization as well as being courteous to use their results in thesis as complimentary support work. I am also thankful to Dr. Jiang and Dr. Hossou for their help and important suggestions during the research work. Also I would like to express my gratitude to the UTA labs centers and lab members as Surface and Nano Engineering Lab (SANEL) and Characterization Center for Materials and Biology (CCMB) to grant me the permission to use the tools and instruments for the research.

I would also be thankful to all my friends for their moral support. Last but not the least; I am deeply grateful to my fiancée Pooja and my parents for all their support and encouragement.

November 16, 2009

ABSTRACT

STRUCTURAL, MAGNETIC AND SURFACE PROPERTIES OF
RF MAGNETRON SPUTTERED UNDOPED
LANTHANUM MANGNITE
THIN FILMS

Varad Rajan Sakhalkar, M.S.

The University of Texas at Arlington, 2009

Supervising Professor: Efstathios I. Meletis

In the present study, polycrystalline and epitaxial undoped Lanthanum Manganite (LMO) thin films were deposited by using RF magnetron sputtering on three substrates, Si (100), MgO (100) and $LaAlO_3$ (100) to study the influence of the misfit strain at the substrate/film interface. The effect of processing conditions on the synthesis of LMO films was studied by conducting deposition on Si wafer. Films were characterized by X-Ray Diffraction (XRD), Atomic Force Microscope (AFM), Energy Dispersive Spectroscopy (EDS) and Superconducting Quantum Interference Device (SQUID) to investigate the influence of processing parameters on their structure and properties. Based on the initial study on Si wafer, processing parameters were selected to deposit LMO thin films on MgO and $LaAlO_3$ substrates. The films were subsequently characterized using XRD, AFM, EDS and SQUID to study the structural, magnetic and surface properties of the as-deposited films as a function of substrate material. Selected films samples were heated at 800^oC in oxygen atmosphere to determine effect of annealing on film microstructure.

XRD results show that the as-deposited films at substrate temperature 750^{o}C exhibited a good quality crystalline structure. On the contrary, the films deposited at 700^{o}C exhibited a rather amorphous like structure. It was also found that the decrease in applied RF power led to better film crystallinity. XRD analysis also revealed that the films deposited on silicon wafer (bare and etched) exhibited a polycrystalline structure and whereas those deposited on $LaAlO_3$ and MgO had a good quality epitaxy. The annealing experiments revealed that the deficiency of oxygen in the as-deposited films was filled by heating at 800^{o}C. AFM results revealed the formation of smooth surface and homogeneous films. SQUID studies showed that the magnetic moment of the films increased with decrease in temperature, below the Neel Temperature. Also, it indicated that the epitaxial films had higher phase transition temperature than the polycrystalline ones. The magnetic phase transition in epitaxial film was found to be 160K, better than reported in previous research. Thus, high quality epitaxial LMO films can be synthesized by RF magnetron sputtering that provides a process for large area deposition.

TABLE OF CONTENTS

ACKNOWLEDGEMENTS....iii

ABSTRACT....iv

LIST OF ILLUSTRATIONS....ix

LIST OF TABLES....xii

Chapter Page

1. INTRODUCTION....1

2. OBJECTIVE....3

3. LITERATURE REVIEW....4

3.1 Perovskite Oxides....4

3.2 Properties of Lanthanum Manganite....6

3.2.1 $LaMnO_3$ Electronic Structure....6

3.2.2 Double Exchange....7

3.2.3 Crystal Structure....10

3.2.4 Electronic Transport....12

3.2.5 Magnetic Properties....13

3.2.6 Colossal Magnetoresistance (CMR)....16

3.3 Substrate Selection....16

3.4 Synthesis Techniques of Epitaxial and Polycrystalline Undoped and Doped Lanthanum Manganite Film....18

3.4.1 Metal Organic Chemical Vapor Deposition....19

3.4.2 Sol-Gel Process....20

3.4.3 Polymer Assisted Deposition....22

3.4.4 Pulsed Laser Deposition 22
3.4.5 Sputtering 26
3.4.5.1 Physics of Sputtering....28
3.4.5.2 RF Sputtering 28
3.4.5.3 Magnetron 29
3.5 Epitaxial and Polycrystalline Thin Film Growth 29
3.5.1 Epitaxy....29
3.5.2 Polycrystalline Film....30
3.5.3 Thin Film Growth 31

4. EXPERIMENTAL DESIGN AND PROCEDURE 32
4.1 Deposition of LMO Thin Films 32
4.1.1 PVD/CVD/Sputtering System 32
4.2 Deposition Procedure 36
4.2.1 LMO Deposition Parameters 36
4.3 Microstructural Characterization....38
4.3.1 X-Ray Diffraction (XRD) 38
4.3.2 Energy Dispersive Spectroscopy (EDS) 39
4.3.3 High Resolution Transmission Electron Microscopy (HRTEM) 39
4.3.4 Surface Properties....40
4.3.5 Magnetic Properties 41
4.3.6 Annealing....42
5. RESULTS AND DISCUSSIONS....43
5.1 Effect of Processing Parameters on Thickness and Deposition Rate of LMO Films 43
5.2. Characterization of $LaMnO_3$ Thin Films 45
5.2.1 EDS Analysis....45

5.2.2 Effect of Processing Parameters on Film Microstructure 45
5.2.2.1 Effect of Substrate Temperature 45
5.2.2.2 Effect of RF Power 47
5.2.2.3 Effect of Silicon Etching.....49
5.2.2.4 Effect of Substrate on Film Microstructure 50
5.2.2.5 Effect of Annealing 53
5.2.3 Transmission Electron Microscopy.....54
5.2.4 Surface Properties.....57
5.2.5 Magnetic Properties 58
6 CONCLUSIONS 63

REFERENCES 64
BIOGRAPHICAL INFORMATION 68

LIST OF ILLUSTRATIONS

Figure Page

3.1 Representation of the Crystal Structure of Perovskite Oxide 5

3.2 Ligand-Field Splitting of Five Fold Generated Atomic 3d Levels Into Lower t_{2g} (Triply Degenerate) and Higher e_g (Doubly Degenerate) levels. Jahn-Teller Distortion of MnO_6 Octahedron Further Lifts Degeneracy 6

3.3 Representation of Double Exchange Mechanism 8

3.4 Types of Spin Alignment in Ferromagnetism a) Ferromagnetism, b) Antiferromagnetism, c) Spin-Canted Antiferromagnetism, d) Defect Anti-ferromagnetism, e)Ferrimagnetism 9

3.5 Variation of the Lattice Parameters and Volume of $LaMnO_3$ with Temperature Under Pressure of 10,15 and 20 kbar 11

3.6 Temperature vs. Resistivity Curve for a Typical Epitaxial $La_{0.67}Ca_{0.33}MnO_3$ 12

3.7 Possible Magnetic Structures of the Perovskite Manganites. The Circle Represents the Mn^+ Ion and the Sign Indicates the Direction of the Projection of the Spin Along Z-Axis 14

3.8 Phase Diagrams of $La_{1-x}Sr_xMnO_3$ (Top) and $La_{1-x}Ca_xMnO_3$ (Bottom). In the Top Diagram Open Circles Show Neel Temperature and Filled Circle Shows Curie Temperature. For the Bottom Diagram Filled Circles are Neel Temperatures and Filled Ones are Curie. Abbreviations Used are As P-Paramagnetic, I- Insulator, F-Ferromagnetic, M-Metallic, CN-Spin Canted, PM-Paramagnetic, FM-Ferromagnetic and AFM- Antiferromagnetic 15

3.9 Preparation Process for $LaMnO_3$ Thin Film and Fine Powder Using Metal Acetylacetonates 21

3.10 Schematic of a Pulsed Laser Deposition (PLD) System 23

3.11 Cross-sectional TEM of (c) LMO/LAO Deposited at 700 °C Showing Continuous Layer (CL) and Nano Column Layer (NCL) Structures. (d) SAED Pattern Taken From the Column Layer in LMO Film 25

3.12 Cross-Sectional TEM Image (c) and (d) SAED Pattern of LMO/LAO Deposited At 800 °C .. 25

3.13 Plan-View TEM of (b) LMO Thin Film Deposited At 700 °C 26

3.14 Schematic of a RF Sputtering System 27

3.15 Schematic of a DC Sputtering System 27

4.1 Schematic Representation of Home Made DC/RF Sputtering System 34

4.2 (a) Front View of the System (b) Side View of the System 35

4.3 Side View of the Sputtering System 36

5.1 XRD Patterns from LMO Films Deposited at 750^{o}C (Film 1) and 700^{o}C (film 4) 46

5.2 Cross Section TEM Micrographs of LMO-Si (a) Film 3, and (b) Film 4 47

5.3 XRD Patterns of Film LMO-Si 1, LMO-Si 2 and LMO-Si 3
Deposited at Different RF Power 48

5.4 Cross Section TEM Micrograph of (a) Film 2 and (b) Film 3 49

5.5 Plan-View TEM Micrograph of (a) Film 2 and (b) Film 3 49

5.6 XRD Patterns from LMO-Si 3 and LMO-S 1 Films
Deposited on Si and Etched Si Wafers 50

5.7 XRD Patterns for LMO Thin Films Deposited on Different Substrates 52

5.8 XRD Patterns for Film LMO-Si3 in the As-Deposited and Annealed Condition 53

5.9 Cross Section HRTEM and SAED Pattern of LMO-Si 3 Film 55

5.10 Cross-Section HRTEM and SAED Pattern of LMO-MgO Film 55

5.11 HRTEM Micrograph of the Interface of LMO-MgO Film 56

5.12 HRTEM Cross Section Micrograph of LMO-LAO Film 56

5.13 (a) Topography and (b) EFM Image of LMO-MgO Film with
Surface Cross Section of 20 μm x 20 μm 58

5.14 Topography (a) and (b) EFM Image of LMO-Si with
Surface Cross Section of 20 μm x 20 μm 58

5.15 Typical Hysteresis Loop Obtained from a LMO Film at Room Temperature 59

5.16 Hysteresis Loop for LMO Thin Films Deposited on Si, MgO and LAO at 10K 61

5.17 Hysteresis Loop for LMO Thin Films Deposited on Si, MgO and LAO at 100K 61

5.18 Temperature Dependent Magnetization for LMO
Thin Films Deposited on Si, MgO and LAO 62

LIST OF TABLES

Table Page

4.1 Parameters for LMO Thin Films Deposition 38

5.1 Processing Conditions and Deposition Rates for LMO Thin Films 44

5.2 Composition Analysis of $LaMnO_3$ Thin Films 45

CHAPTER 1

INTRODUCTION

The introduction of nanotechnology has captivated the world by its extent of application in handheld electronics, biotechnology, medical applications to space and energy. Materials science has played a large role in this era by the invention of nanomaterials, of completely new properties, used in all these applications.

Perovskite oxides have been studied from the early 1950's[1] for their interesting physical properties like double exchange mechanism, electronic transport properties as well as magnetic properties. But the major break through in the research of these materials came in early 1990's[1] with the discovery of colossal magnetoresistance (CMR). Following that, the interest in the field of perovskite oxide materials was refueled. With the ongoing research, some very exciting properties of the perovskite oxides, especially CMR-manganites, were discovered like spin electronics, half metallicity, Hall Effect, charge ordering, superconductivity and high thermo power. These newly discovered properties have generated interest in these materials, especially in the direction of applications in sensors, actuators and devices.

Thin films of lanthanum manganite (LMO-$LaMnO_3$) exhibit very different structural, magnetic and electric properties than their bulk counterpart. Doping of basic lanthanum manganite has improved the magnetic and electric properties of the manganites. The films deposited at elevated temperatures show perovskite cubic[2] structure due to a phase change apart from bulk material, which is rhombohedral and orthorhombic[3] at room temperature. Many researchers have previously reported on the synthesis of doped lanthanum manganites with strontium, calcium and sodium. Doping of lanthanum manganite with strontium up to 20 % has

promoted the ferromagnetic phase transition at room temperature[4-5]. The substitution of 33% of lanthanum by barium atoms has exhibited the occurrence of 60% of colossal magnetoresistance at 5 Tesla applied field at room temperature[4]. Doping of different elements enabled the utilization of these materials in applications as magnetoresistive sensor as well as bolometer.

To understand the physics behind the doped lanthanum manganites, it is necessary to study the undoped lanthanum manganite first. The thin films of undoped lanthanum manganites had been studied to understand the science behind newly discovered properties of doped manganites. Previous research on these thin films[5, 6, 7, 8] show that the deposition technique is critical in the synthesis of thin films of lanthanum manganites for their desired structure and properties. Also, there has been ongoing research to develop a low-cost and effective deposition system that will enable synthesis of these films with better control and savings in processing. Up to date, many researchers have reported synthesis of lanthanum manganite thin films with wet techniques like sol-gel[7], polymer assisted deposition[9] and dry processes like MOCVD[6] and pulsed laser deposition[2] (PLD). Each process has its own advantages and disadvantages. Along all these deposition techniques it was reported that dry processes like PLD and sputtering are producing better results, in terms of film quality, for synthesis of epitaxial thin films.

Meletis and co-workers[2] has shown that, during pulsed laser deposition, temperature can be a very crucial parameter that can affect film microstructure entirely. They have reported the growth of self textured columnar structure on the top of continuous epitaxial layer of lanthanum manganite at a specific deposition temperature.

The major disadvantage of PLD is that it is not effective for deposition on large surfaces. In this study, the synthesis of undoped lanthanum manganite ($LaMnO_3$) or LMO thin films has been explored using RF magnetron sputtering technique. The use of RF power along with use of magnetron has the potential to cause an enhancement in density and uniformity of plasma and thus more effective deposition. Furthermore, it is well established that, the film growth is significantly affected by the underlying substrate material. Thus, the aim of this work was to investigate the effect of RF power on structure of the films as a function of underlying substrate.

CHAPTER 2

OBJECTIVE

The goal of the present study was to explore the deposition of LMO thin films by utilizing RF magnetron sputtering process on various substrates. Three substrates were selected in order to influence the misfit strain at the substrate/film interface, with the expectation to synthesize epitaxial LMO films as lanthanum aluminate ($LaAlO_3$), magnesium oxide (MgO) and silicon.

The main objectives of this research work were;

(i) to determine the effect of various processing parameters as RF power, temperature and pressure on growth of LMO thin films.

(ii) study the effect of the substrate material (misfit strain) on the characteristics of LMO thin films.

(iii) study the electric, magnetic and surface properties of produced LMO thin films.

CHAPTER 3

LITERATURE REVIEW

Lanthanum manganite represents a class of perovskite oxide materials. In recent times, perovskite oxide materials drew a lot of attention due to their intriguing and interesting properties like colossal magnetoresistance, ferroelectricity, superconductivity, charge ordering spin transport, thermopower and the variation in these aforementioned properties according to change in their crystalline structure. Hence, to understand the properties of LMO, an overview of perovskite oxide structure is needed.

3.1 Perovskite Oxides

Perovskite is a group of materials that represents similar crystal structure as its prototype calcium titanium oxide, $CaTiO_3$. Perovskite minerals were first discovered in Ural Mountains of Russia and were named after Russian mineralogist L. A. Perovski. Perovskite-type materials can be represented by their general formula as ABX_3 where, A and B are any two different sized cations and B is the anion bonding them. Most of the perovskites contain oxygen as the anion. Hence, perovskite oxides can be presented by their general formula as ABO_3. In perovskite oxides, the A ion can be a rare earth element, alkali element or other large ion like Pb^{2+}, Bi^{3+}; which can fit into the dodecahedron frame and B ions can be 3d, 4d or 5d transition metal ions placing themselves at the octahedral sites as shown in Figure 3.1

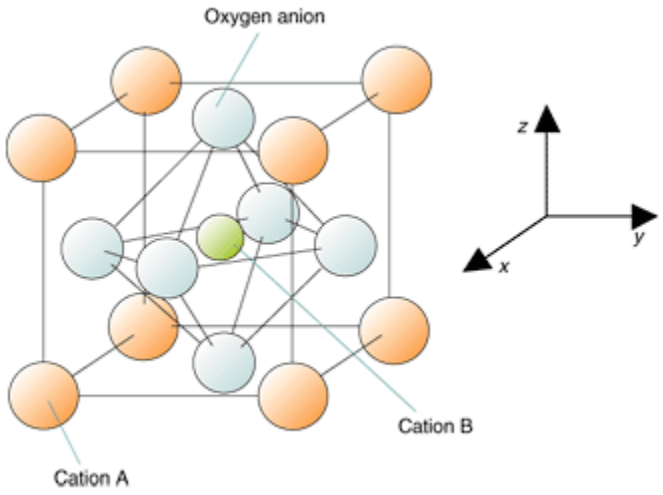

Figure 3.1 Representation of the crystal structure of perovskite oxide.

Generally, perovskite oxides can only be formed if the tolerance factor, T, ranges between 0.8-1.0[10]. The tolerance factor, T, is given by

$$T= (R_a+R_o) /\sqrt{2}\ (R_b+R_o) \qquad (3.1)$$

where, R_a and R_b are the atomic radii of A and B cations and R_0 is the ionic radius of oxygen. Ideal perovskite oxides have all the atomic states filled. Electrons cannot move freely through the crystal as the atoms are bonded with strong ionic bonds. This makes the perovskite electrically insulating. Also, perovskites are cubic and isotropic. The unusual and interesting properties of perovskite oxides, as mentioned before, come into play when there is distortion in lattice structure differing from the ideal one. If the tolerance factor, T, is differed from its range, i.e., if the radius of ion A is very large compared to ion B, then, the octahedral structure of B ions gets tilted leading to the distortion in lattice. The symmetry of the lattice gets affected resulting in altering the electrical, optical, elastic, magnetic properties. Some tilted perovskites contain a B atom at the center of their octahedron structure. In some other perovskites, the position of B cations is shifted resulting in ferroelectricity due to electric polarity of the crystals. $BaSrTiO_3$ can be an example of this type.

Properties of the perovskite also can be varied by substituting either A or B ions with different ions. Lanthanum strontium manganite ($La_{1-x}Sr_xMnO_3$) is one example where A cation lanthanum is substituted by strontium. PZT is an example of replacement of B cation where some amount of titanium is replaced by zirconium.

3.2 Properties of Lanthanum Manganite

3.2.1 $LaMnO_3$ Electronic Structure

$La^{3+}Mn^{3+}O_3^{2-}$ is the chemical formula for undoped lanthanum LMO. The Mn^+ ion is surrounded by oxygen octahedron. The 3d orbitals on Mn^+ site are placed as such an octahedral coordination is subject to the partial lifting of the degeneracy by the crystal field, as shown in Figure 3.2

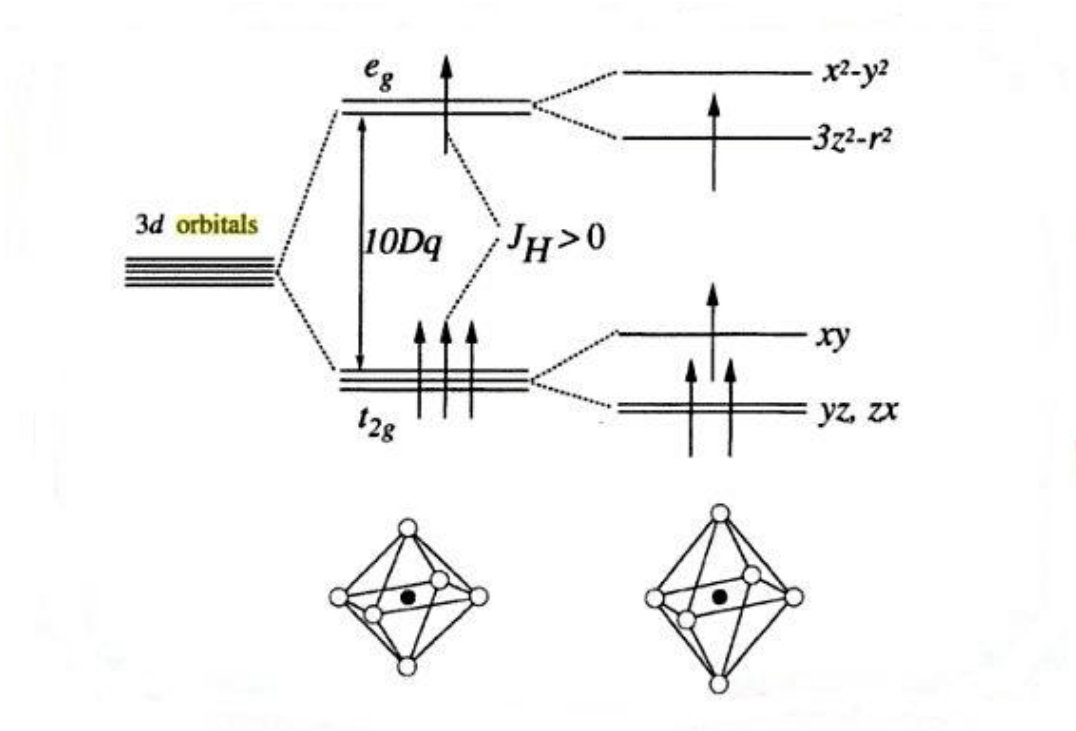

Figure 3.2 Ligand-field splitting of five fold generated atomic 3d levels into lower t_{2g} (triply degenerate) and higher e_g (doubly degenerate) levels. Jahn-Teller distortion of MnO_6 octahedron further lifts degeneracy.

The lower lying orbitals, t_{2g} states, are d_{xy}, d_{yz} and d_{zx}; while the higher lying one, e_g, are d_{x2-y2} and $d3_{z2-r2}$. The crystal field splitting between e_g and t_{2g} states is about 1 eV. The e_g orbitals are oriented towards the neighboring oxygen atoms while t_{2g} states have nodes in that direction suggesting that only e_g orbitals can intermix with oxygen p orbitals[4].

According to Hund's rule, all the d electrons on a Mn^{+} ion must have same spin means; all the three electrons in the t_{2g} states will have the same spin. Also, one electron in e_g state should also have same spin as in electrons in t_{2g} state. Also, Jahn-Teller effect should have considered here for the distortion of the crystal. Jahn-Teller theorem states that, any non-linear molecular system in a degenerate electronic state will be unstable and will undergo distortion to form a system of lower symmetry and lower energy, thereby removing the degeneracy. With an electron in the e_g state, this will lower the energy of the system[4].

3.2.2. Double Exchange

The correlation between the electrical conductivity and ferromagnetism was introduced by Jonker and Van Santen[12] through the theory of double exchange proposed by Zener[13]. This theory predicts that, an electron may be exchanged between two species and has important implications for whether materials are ferromagnetic, antiferromagnetic or neither with relative ease. In the double exchange phenomenon Mn^{3+}-O-Mn^{4+} and Mn^{4+}-O-Mn^{3+} bonds degenerate leads to delocalization of the electron on Mn^{4+} site. The delocalization of electron at Mn^{4+} site lowers the energy of system and there is an energy gain by aligning the t_{2g} spins. The delocalization of electron at Mn^{4+} site can be shown as Figure 3.3

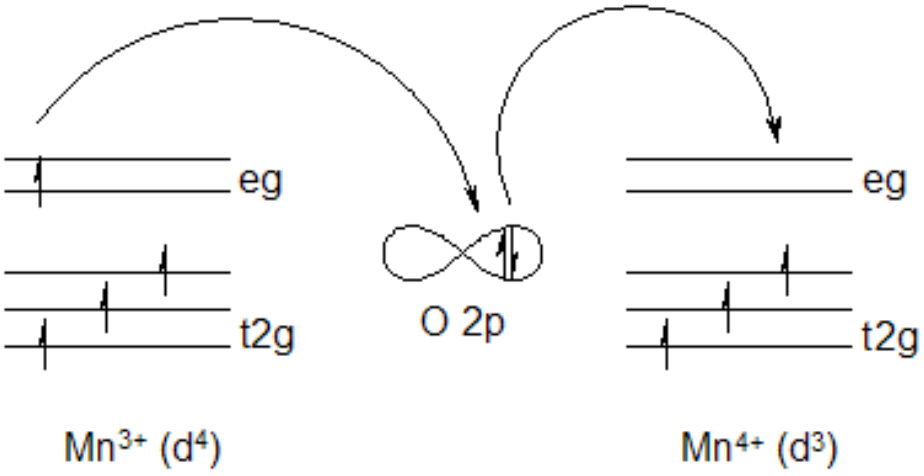

Figure 3.3 Representation of Double Exchange Mechanism

Undoped LMO is an insulator at room temperature because all Mn^{+} ions have one electron in the lower e_g level. An electron needs to go to the higher e_g level to move from Mn^{3+} site to Mn^{4+} site. Under the Neel temperature, the energy of this barrier lowers and the spin canted ferromagnetism is induced in LMO. In ferromagnetism (Figure 3.4 a), the exchange energy is minimized when all the spins are parallel as occurs in pure iron. When spins are perfectly antiparallel (antiferromagnetism, Figure 3.4b), there is no net magnetic moment, as occurs in ilmenite. Occasionally, the antiferromagnetic spins are not perfectly aligned in an antiparallel orientation, but are canted by a few degrees. This spin-canting (Figure 3.4 c) gives rise to a weak net moment, as occurs in hematite, a common magnetic mineral.

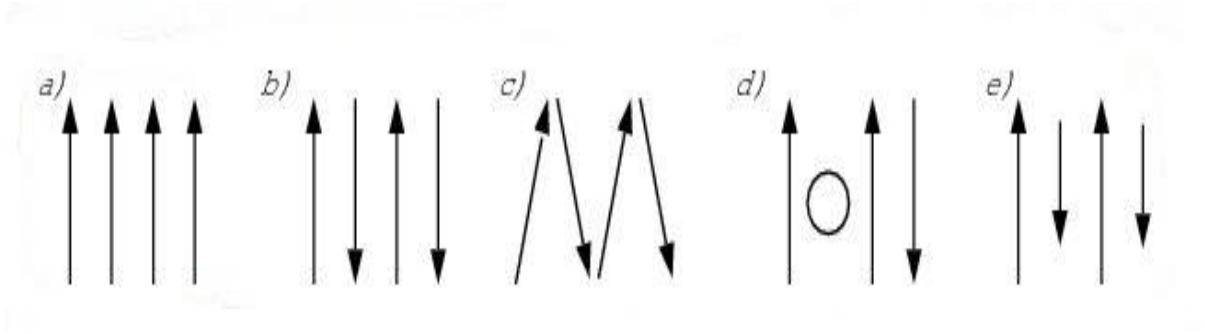

Figure 3.4 Types of spin alignment in ferromagnetism a) ferromagnetism, b) antiferromagnetism, c) spin-canted antiferromagnetism, d) defected anti-ferromagnetism, e) ferrimagnetism.

As doping percentage in LMO increases, more numbers of Mn^{3+}- Mn^{4+} pairs will lead to ferromagnetism. The relationship between electrical conductivity and percentage of Mn^{4+} was given by Zener[13] as,

$$\sigma = (xe^2/ah)\ (T_c/T) \qquad (3.2)$$

where, T is temperature, 'T_c' is Curie temperature, 'a' is lattice parameter and 'x' is fraction of Mn^{4+} ions.

The Mn-O-Mn bond is not usually ideal 180^0, as the perovskite structure is not perfect. The bond length and bond angle plays a major role in the manganites properties like magnetism and conductivity. Batlogg and coworkers[14] showed that, it is possible to vary the ionic radius of the ion at A-site perovskite by using different trivalent rare earth element ions. Their experiments shown that, with increase in radius of A-site ion, temperature for metal insulator transition, T_{mi} also increased. By increasing the A-site radius, the rotations of the octahedrons become smaller and Mn-O-Mn bond angle close to 180^0. Zhang and coworkers[15] compared the effects of applying external pressure to undoped LMO to the application of phase change and the change in lattice parameter and lattice structure. They showed that, application of external pressure of 10 kbar and 15 kbar leads to phase transition in undoped LMO and transition temperature varies with the amount of pressure applied, as shown in Figure 3.5. The decrease in cell volume caused by the isostatic pressure will reduce the ionic size mismatch, which will decrease the rotation of oxygen octahedrons getting θ closer to 180^0.

3.2.3. Crystal structure

The ideal structure of lanthanum manganite is perovskite cubic with lattice parameter a = 0.387 nm. If there is a deviation from the difference in radii of A and B site ions (Goldschmidt Tolerance Factor), then new unit cell will be of different type due to change in crystal symmetry. Coey and Viret[16] showed that, the Jahn-Teller effect causes distortion by elongating oxygen octahedron in some direction. Also, with a lager misfit of ionic sizes, there will be buckling of MnO_6 octahedron to an orthorhombic structure. The thin films structure of lanthanum manganite depends upon substrate crystal structure as well as film processing parameters.

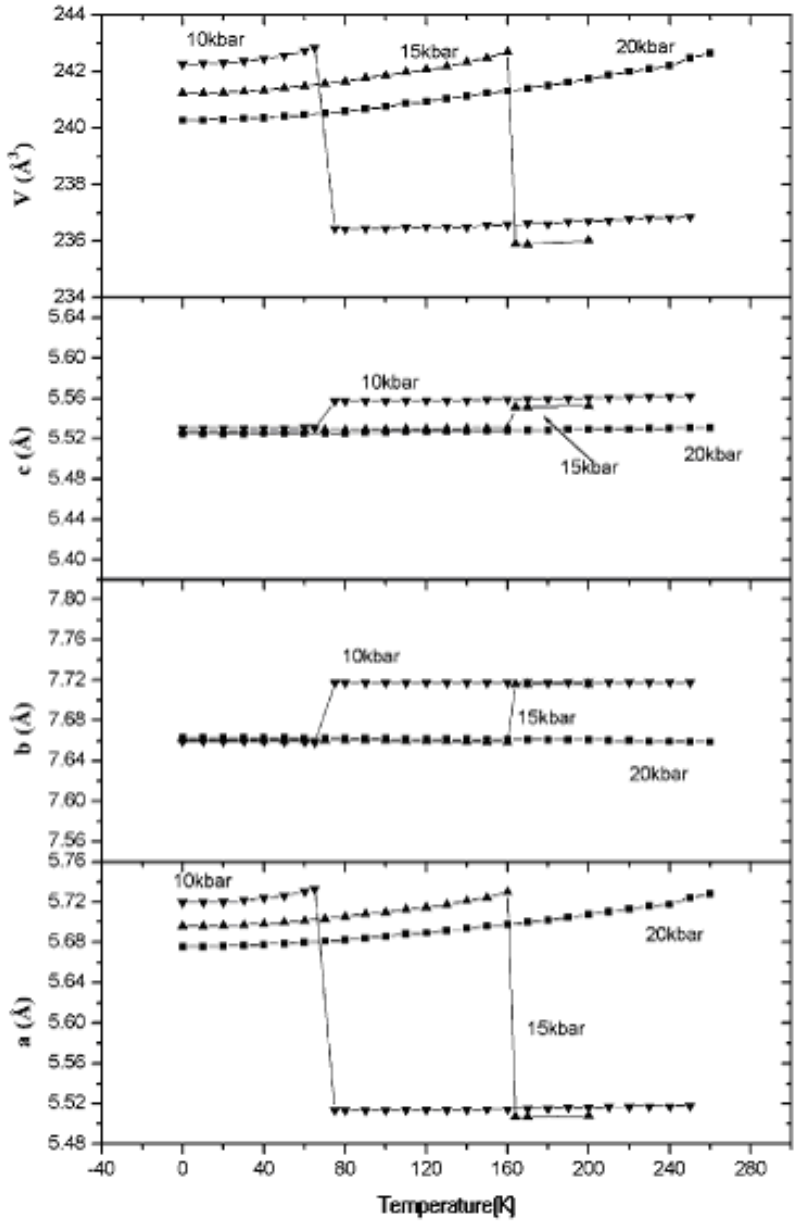

Figure 3.5 Variation of the lattice parameters and volume of $LaMnO_3$ with temperature under pressure of 10, 15 and 20 kbar.

3.2.4. Electronic Transport

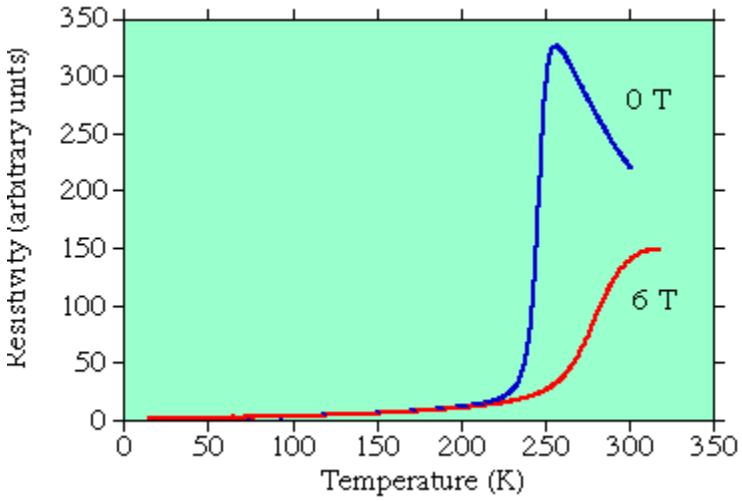

Figure 3.6 Temperature vs. Resistivity curve for a typical epitaxial $La_{0.67}Ca_{0.33}MnO_3$.

The resistivity vs. temperature curve for typical calcium doped LMO is as shown in the Figure 3.6. The curve shows two distinct regions. The region at the lower temperatures, showing increase in resistance with temperature and the region at high temperature showing decrease in resistivity with temperature. Below the peak resistivity the sample shows the metallic behavior and semiconducting above. The sample is ferromagnetic in the metallic region and paramagnetic in the semiconducting region. Temperature at the maximum slope is called as the transition temperature, T_{tr} as this temperature is close to the ferromagnetic ordering temperature T_c.

For the temperature vs. resistivity curve, the resistivity, plotted as log p versus 1/T follows straight line, showing activated behavior,

$$p\ (T)\ \alpha\ e^{E_0/kT} \qquad (3.3)$$

where e_0 is the activation energy and k is Boltzmann constant in the paramagnetic region[12]. In the ferromagnetic region, the resistivity has been found to be described as

$$p\ (T) = p_0 + AT^2 + BT^{4.5} \qquad (3.4)$$

Kubo and Ohata[17] in their work showed that the term $T^{4.5}$ is caused by two magnon process. Since the charge carriers at low temperature are spin-polarized, first order spin-wave interactions will decrease exponentially with temperature. Such processes would give a T^2 behavior of the resistivity. Therefore it has been suggested that the T^2 term comes from electron-electron scattering.

3.2.5. Magnetic properties

Wollan and Koehler[18] first studied the neutron diffraction measurements on a series of $La_{1-x}Ca_xMnO_3$ samples. The samples showed the various antiferromagnetic and ferromagnetic kinds of behaviors, depending upon the level of calcium doping. The different magnetic structures they observed are as shown in Figure 3.7. The $LaMnO_3$ was found to be antiferromagnetic (labeled A in the Figure 3.8) with ferromagnetic planes that had alternating directions of magnetization. The 100% doped $CaMnO_3$ was also found to be antiferromagnetic.
Mn^{4+} ions are surrounded by the six closest neighbors having opposite spin (label G). Other doping levels gave other types of antiferromagnetic ordering, but in the doping range of x=0.3 the samples were ferromagnetic (label B).

Shiffer and coworkers[19] studied measurements of the magnetic states of manganites as a function of temperature and doping in $La_{1-x}Ca_xMnO_3$ ceramic samples. Urushibara and coworkers[20] measured it for $La_{1-x}Sr_xMnO_3$ single crystals. These phase diagrams are shown in Figure 3.9. The CMR effect takes place at the ferromagnetic to paramagnetic transition, with a doping level approximately between 20 and 50%. The maximum Curie temperature is achieved with a doping level of around 30%. Goodenough and Loeh[21] have explained the magnetic structures for different doping levels in terms of different types of bonding, where some bonds are ferromagnetic and others are antiferromagnetic or paramagnetic. This is determined by the relative orientation of occupied and unoccupied orbitals of the Mn-O-Mn pairs.

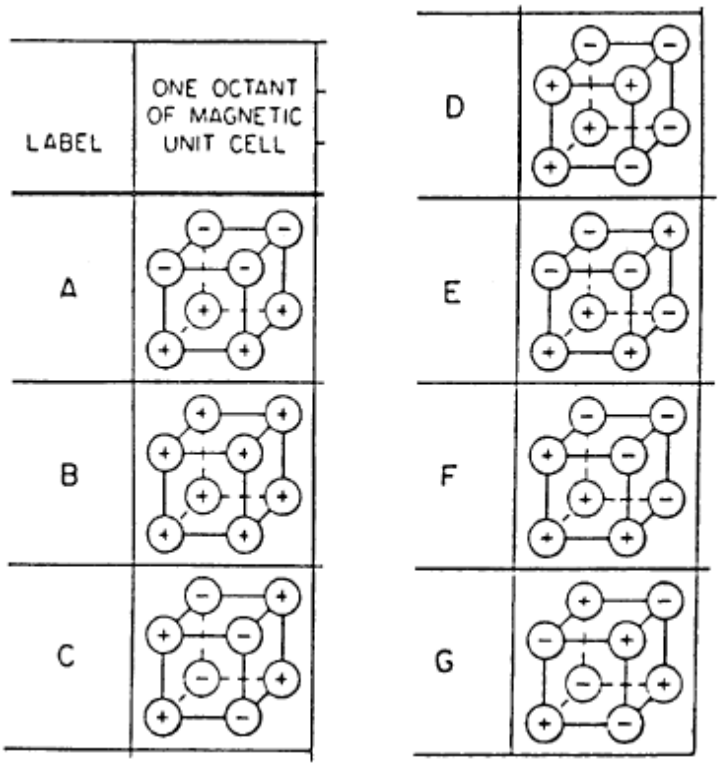

Figure 3.7 Possible magnetic structures of the perovskite manganites. The circle represents the Mn^{+} ion and the sign indicates the direction of the projection of the spin along z-axis.

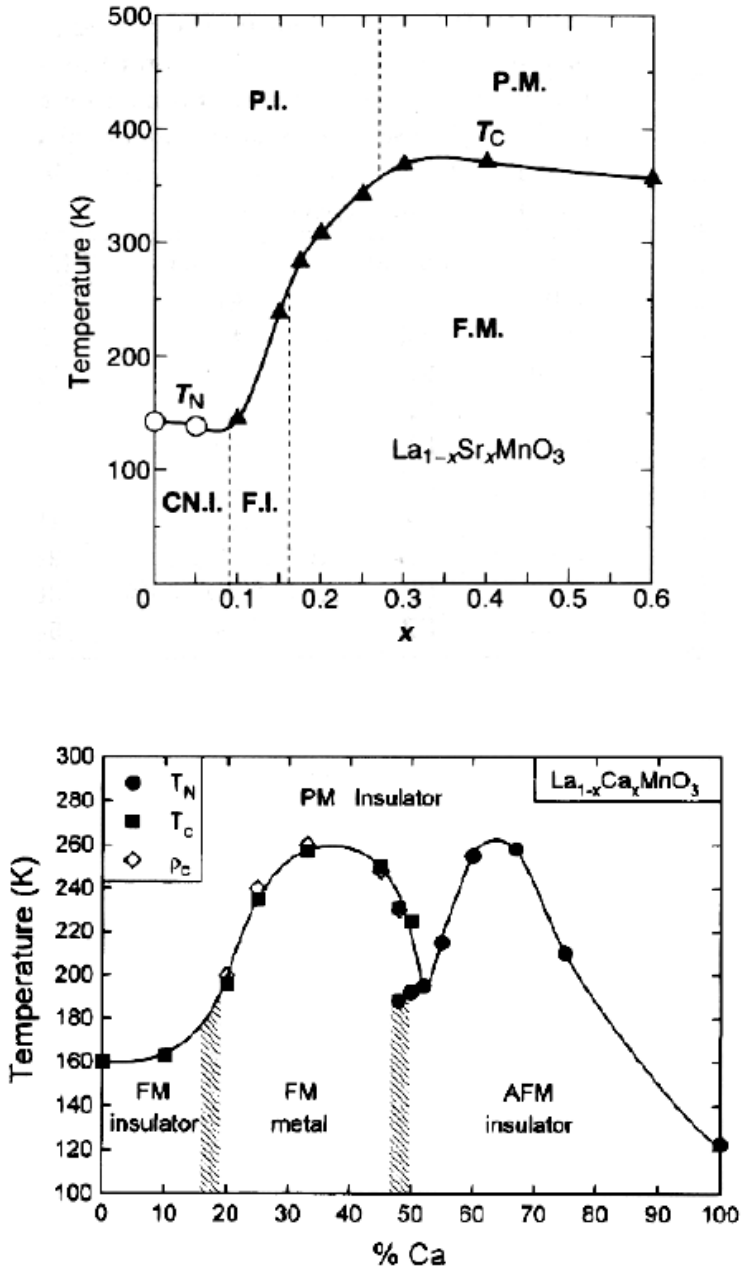

Figure 3.8 Phase diagrams of $La_{1-x}Sr_xMnO_3$ (top) and $La_{1-x}Ca_xMnO_3$ (bottom). In the top diagram open circles show Neel temperature and filled circle shows Curie temperature. For the bottom diagram filled circles are Neel Temperatures and filled ones are Curie. Abbreviations used are as P-Paramagnetic, I- insulator, F-Ferromagnetic, M-Metallic, CN-Spin Canted, PM-Paramagnetic, FM-Ferromagnetic and AFM- Antiferromagnetic.

3.2.6. Colossal Magnetoresistance (CMR)

Colossal magnetoresistance is a materials property which enables it to change its electrical resistance in the presence of magnetic field. A magnetic field applied to perovskite manganite in the paramagnetic semiconducting state, enables its phase transformation into ferromagnetic metallic state causing colossal magnetoresistance to occur. The magnetoresistance has a peak close to position of the maximum slope of the resistivity curve. There should be a large change of resistivity with temperature to have a large magnetoresistance. Also the transition temperature should be highly sensitive to the applied field.

The double exchange phenomenon helps to explain the CMR effect. The applied magnetic field will align the t_{2g} spins and the transport will be possible between Mn^{+} ions. At the Curie temperature both spin will disorder and magnetic susceptibility will be high that maximizes the effect of applied field.

In order to have a sharp transition between the metallic and insulating state, the sample should be as homogeneous as possible so that all parts have the same transition temperature. If there are polycrystalline grains, there will be regions between the grains that have different transition temperatures because the material is distorted with different Mn-O-Mn bond angles and lengths and different Mn^{4+} concentrations. The resistivity curve for the whole sample is a superposition of the resistivity curves for the different parts, and with different transition temperatures there will be a broader transition.

3.3 Substrate Selection

Selecting a substrate for deposition of thin films is at most important factor which dictates not only the quality of deposited film, but also the feasibility of growth of the film. When selecting a substrate for thin film deposition, the substrate should provide mechanical support only, rather than interact with the film except from sufficient adhesion. It should also act as a template for atomic ordering[22].

There are a number of parameters that are critical while selecting the substrate, that can affect the growth and quality of the film,

1. Chemical compatibility:

   While depositing an epitaxial or polycrystalline film, the necessary precaution should be taken that, the chemical composition of the substrate should be suitable to that of the film. There should not be any chemical reaction between those two. Also, if the LMO films are grown in the oxygen atmosphere, the substrate should not react with oxygen.

2. Thermal expansion match/mismatch:

   Thermal mismatch between substrate and film can rise to cracking of the film. If the film is ceramic, then the brittleness of the film enhances the chances of cracking effects. If the mismatch is large, then the thicker films can break easily due to strain.

3. Surface morphology:

   The quality of the surface is one of the most important properties of a substrate as the surface is the place where film interacts with substrate. The uniform surface ensures a homogenous and uniform film. If the surface is not regular, there are many defects can be seen in the film as point defects, dislocation lines, twin boundaries, pores, surface wraps, cracks etc. An ideal surface should have a flat, dense surface which is free from twins.

4. Thermodynamic stability:

   The substrate should not undergo any phase at the given temperature during the deposition of the film. The lanthanum manganite films are generally deposited over the temperature of 500^0C hence at such high temperature the substrate structural and morphological properties should remain stable. This property is very important for deposition of epitaxial films.

There are some additional factors that also contribute when growing epitaxial films. For growing epitaxial films, there should be certain relation between the crystallographic orientation of substrate and film.

1. Lattice mismatch:

   To get a good quality epitaxial film the in plane lattice parameters difference between the film and substrate should be minimum. The large difference between lattice parameters of substrate and the film can lead to the breaking of the film after a certain thickness due to the strain exerted by the mismatch.

2. Coincide sites:

   Along with the minimum difference between the lattice parameters, the atoms coincide should have the same valencies and preferably same radius.

3. Surface quality:

   Surface quality factor is more important in growing epitaxial films than polycrystalline as misoriented grains often nucleate on irregularities of the film.

The lattice parameter of perovskite cubic structured lanthanum manganite is 3.95 Å. Hence, to grow the epitaxial films of LMO, magnesium oxide (MgO) and lanthanum aluminate ($LaAlO_3$ or LAO) substrates were selected. LAO has the rhombohedral structure with lattice parameter as a= 3.79 Å and c= 13.11 Å. It has the cubical structure above 435^0 C with lattice parameter as a= 3.821 Å. As LMO films were deposited above 700^0C, LAO has the similar crystal structure that of film. On the other hand, MgO has a cubic structure with the lattice parameter a= 4.21 Å. These two substrates have very high melting point than the deposition temperature and there is no phase change during deposition of the film. As per the calculation of lattice mismatch, the film deposited on lanthanum aluminate will be strained in tension and the film deposited on the MgO substrate would be strained in compression.

3.4 Synthesis Techniques of Epitaxial and Polycrystalline Undoped and Doped Lanthanum Manganite Film

The study of properties of perovskite oxide materials has started in 1950s[12] but the interest in these materials was lit up in late 90's when it was found that the thin films of perovskite materials showed very different properties than that of bulk. The renewed interest on the doped

and undoped manganites came out from the observation of a high magnetoresistive effect, designed as “colossal” (CMR), which triggered the attention of the scientific community both for the fundamental research and for the applicative possibilities, particularly for the spin-dependent transport devices.

Successful synthesis of doped and undoped LMO films using different processing techniques and different substrates has been reported[5,6,7,8]. The most popular processing techniques used are the dry processes like PLD, MOCVD and DC and RF Sputtering and wet processes like sol-gel method and polymer-assisted deposition. Each process has its advantages and disadvantages. As the vacuum processes like sputtering and pulsed laser deposition has high infrastructure as well as high operation and maintenance cost but the quality of the films is superior and processing is easier compared to wet processes. The wet process like sol gel synthesis is a low cost process but the processing is difficult and the quality of the films is inferior to films synthesized by vacuum processes.

3.4.1. Metal Organic Chemical Vapor Deposition

In metal organic chemical vapor deposition method, the atoms of the elements (here the atoms of Lanthanum and Manganese) are combined with the complex organic gas molecules (here for e.g. 2,2,6,6-tetramethyl 3,5-heptanedione)[6] and passed over the hot substrate. The heat breaks up the molecules and deposits the desired atoms on the surface, layer by layer. By changing the composition of the gases, the composition of the film can be changed. The possible disadvantages of this method are the exhaust fume is poisonous and difficulty in getting desired stoichiometry. Also MOCVD has problems with obtaining volatile precursors of adequate long term stability.

Senateur and coworkers[23] reported the synthesis of epitaxial Lanthanum LMO thin films on $SrTiO_3$, MgO and $LaAlO_3$ substrates using MOCVD method. The deposition temperature was 600^0C and the samples were annealed in oxygen atmosphere at 700^0C. They reported that the epitaxial films synthesized had the deficiencies of both Mn and O ($La_{1-x}Mn_xO_{3-\partial}$ structure). They also reported that, although all the samples deposited on different substrates exhibited epitaxy,

the film deposited on $SrTiO_3$ produced the best interface match due to having least lattice misfit between substrate and film. They also stated that the non-stoichiometry of lanthanum manganite film played an important role in altering the magnetic and electrical properties. They have reported the magnetic transition temperature as 276K due to the heat treatment of the films in the oxygen atmosphere and non-stoichiometry, which is ideally around 130-150K.

In the synthesis of LMO thin films on RABiTS (Rolling-Assisted biaxially textured substrates) Ni, Kaul and coworkers[6] achieved the synthesis of polycrystalline LMO thin films in the presence of ammonia and water vapor atmosphere by the MOCVD method. They also found that the films deposited in the absence of the particular atmosphere showed individual lanthanum oxide (La_2O_3) and manganese oxide (Mn_2O_3) instead of any formation of LMO.

3.4.2. Sol-Gel Process

Sol-gel process is a widely used wet chemical technique to fabricate materials, starting from a chemical solution, which acts as a precursor for an integrated network called gel of either discrete particles or network polymers. Typical precursors are either metal alkoxides or metal chlorides, which undergo various forms of hydrolysis and polycondensation reactions. The formation of a metal oxide involves connecting the metal centers with oxo (M-O-M) or hydroxo (M-OH-M) bridges, therefore, generating metal-oxo or metal-hydroxo polymers in solution. Thus, the sol evolves towards the formation of a gel-like diphasic system containing both a liquid phase and solid phase whose morphologies range from discrete particles to continuous polymer networks. The advantage of this process is that it is very cheap in operation i.e. low foundation, operation and maintenance cost. The disadvantages are the problems in getting stoichiometry, difficulty in controlling reaction rates, concentration etc.

Murata and coworkers[7] reported the synthesis of LMO thin films using sol-gel method. The preparation process of LMO using sol-gel method is as shown in Figure 3.9.

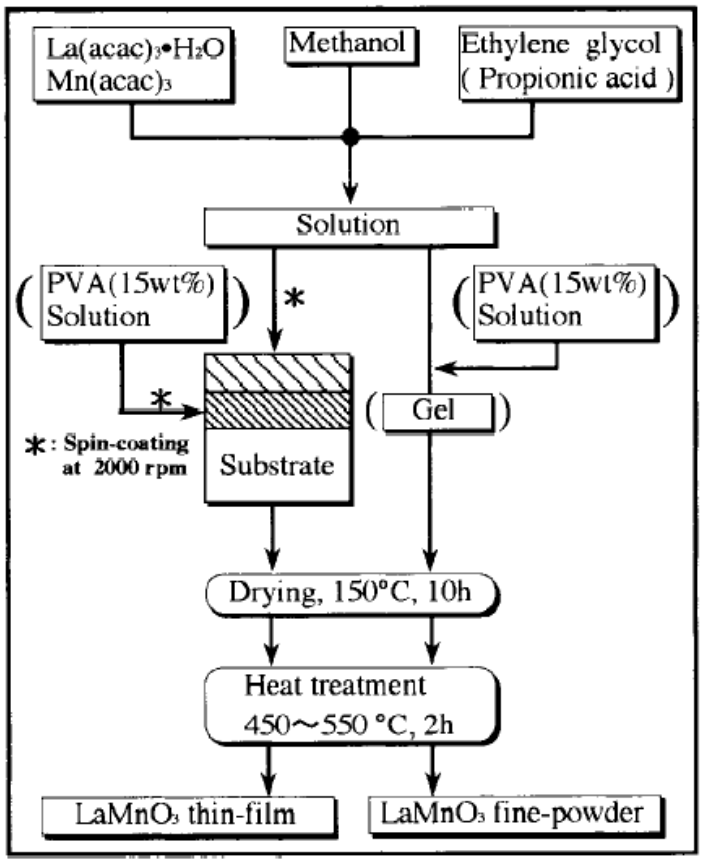

Figure 3.9 Preparation process for $LaMnO_3$ thin film and fine powder using metal acetylacetonates.

They reported the synthesis of polycrystalline LMO films on quartz by spin coating, which were subsequently heat treated at 400-500^{0}C.

Kumagai and coworkers[8] have reported the synthesis of LMO thin films by combined laser ablation chemical solution deposition, excimer laser-assisted metal organic deposition (ELAMOD) method. They found that the films deposited showed polycrystalline, textured and epitaxial structures on strontium titanate ($SrTiO_3$). The formation of these structures was a result of the difference in the pulse times of the excimer laser. The small pulses of laser formed the amorphous structure while the formation of the epitaxial films was mainly due to large pulses of excimer laser.

3.4.3. Polymer Assisted Deposition

Mccleskey and coworkers[9] reported the synthesis of lanthanum strontium manganite ($La_{0.67}Sr_{0.}33MnO_3$ or LSMO) and lanthanum calcium manganite ($La_{0.67}Ca_{0.33}MnO_3$ or LCMO), by using polymer assisted deposition process, a modification in the sol-gel process. The major distinction between PAD and sol-gel process is the functionality of the polymer used in the solution. In the PAD, the polymer has dual functions. Soluble polymer in the solution helps in achieving desired viscosity as well as functions as a binding agent to the metal precursor, which makes it possible to grow crack-free epitaxial films of both simple and complex metal oxides. They deposited the LSMO and LCMO films using spin coating technique of respective precursors of the metal with prepared separately with a polyethyleneimine (PEI) polymer and ethylenediaminetetraacetic acid on $LaAlO_3$ substrate. They reported that the films synthesized have the epitaxial structure. They also studied the effect of different annealing temperature on crystallinity, microstructure, magnetic, and magnetoresistance properties. They stated that the films annealed at lower temperature showed 20% magnetoresistance which is diminished in the films annealed at high temperature.

Even though the wet chemical processes have their distinct advantages of low cost, the dry processes like pulsed laser deposition and sputtering have been extensively used to synthesize and study the doped and undoped LMO films because of desired stoichiometry, good reproducibility, easy control over the processing parameters and the purity of films.

3.4.4. Pulsed Laser Deposition

PLD is a thin film deposition technique, where a high powered pulsed laser beam is focused in a vacuum chamber on the target of material to be deposited. The material is then vaporized to deposit on the substrate facing the target, as thin film. The process is either carried out in ultra high vacuum or desired gaseous atmosphere. The advantages of PLD are the possibility of congruent transfer of even complex materials, versatility of the process as the laser

wavelength below 250 nm, any material can be ablated, simplicity of the process and easy synthesis of multilayered films. The main disadvantages are that the process is not good for deposition of the films on large surfaces (>1 cm^2), high capital cost and possible small defects seen in the film. The schematic construction of a PLD system can be shown as figure 3.10.

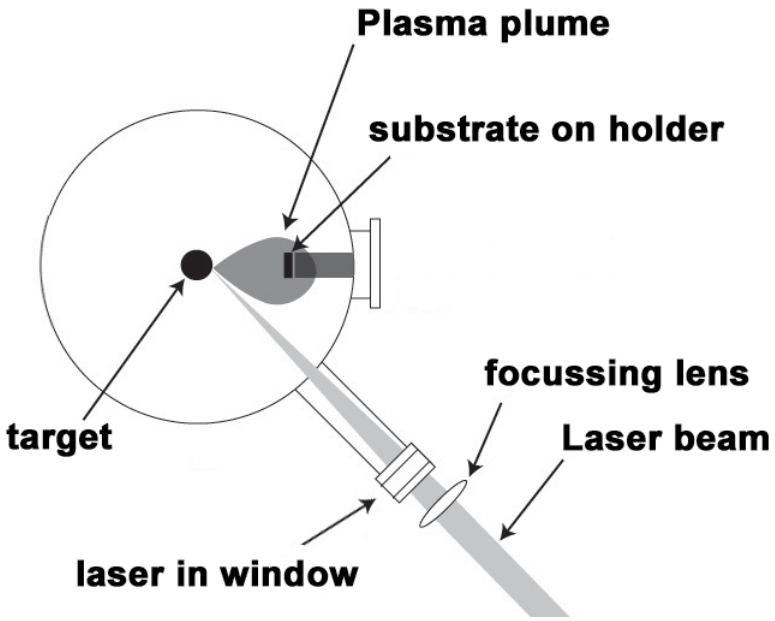

Figure 3.10 Schematic of a Pulsed Laser Deposition (PLD) system.

Ko and coworkers[24] reported the synthesis of LMO thin films by using PLD method on IBAD-MgO substrate. They reported that the deposited film showed the epitaxial structure. They studied that the in plane texture of LMO buffer layers were sensitive to deposition temperature as well as the deposition time i.e. layer thickness.

Aruta and coworkers[25] reported the epitaxial growth of $LaMnO_{3-\delta}$ thin films on $SrTiO_3$ substrate with lattice parameter 3.99 Å. They investigated the magnetic phase transition temperature for LMO thin films was 131K.

Gupta and coworkers[26] reported the fabrication of lanthanum deficient LMO thin films on $SrTiO_3$ substrate by pulsed laser deposition. They showed that, the deficiency of cation plays an

important role in the magnetic, electric and magnetoresistive properties of the thin plays an important role in the magnetic, electric and magnetoresistive properties of the thin films. They found the existence of large magnetoresistance in ferromagnetic $La_xMnO_{3-\delta}$ films at room temperature. The increase in lanthanum deficiency leads to increase in T_c of as deposited films. The magnetoresistance increase with the applied field and was found to be maximum near T_c.

Chen and coworkers[27] studied the effect of substrate dependence on microstructure and magnetoresistance on lanthanum deficient lanthanum manganite thin films. They synthesized polycrystalline La deficient lanthanum manganite thin films on silicon and yttria stabilized zirconia (YSZ) substrates. They reported that, LMO buffer layers deposited on YSZ improved the crystallinity and magnetization of the films compared to that of deposited on silicon.

Meletis and coworkers[2] reported the composition and growth-temperature effects on microstructure of lanthanum manganite thin films deposited on (001) $LaAlO_3$ substrates by pulsed laser deposition. They reported that, at certain temperature (700^0C) the formation of the columnar structure takes place on the top of the continuous epitaxial layer of LMO, while there is only formation of continuous epitaxial layer at other temperatures. The structure of the epitaxial layer was perovskite cubic, while the structure of the columnar layer was orthorhombic as shown in Figures 3.11, 3.12 and 3.13. Shchukin and coworkers[28] theoretically described that, such an ordered array of orthogonal nano columns of continuous, coherently strained layers may spontaneously form stable, periodic; three dimension arrays of equal sized islands, under certain conditions. Some of the strain arising from the film/substrate lattice mismatch is released at the interface by forming crystallographic defects. However, the total strain energy increases with film thickness and at a certain critical value the energy associated with the formation of crystallographic column faces is smaller than the total strain energy and the structure breaks up into columns.

The other popular thin film deposition technique is sputtering. Park and coworkers[29] have reported the deposition of Ca and Sr doped LMO thin films using both RF and DC sputtering. The main advantage of sputtering is that the deposition can be carried out on a large surface area.

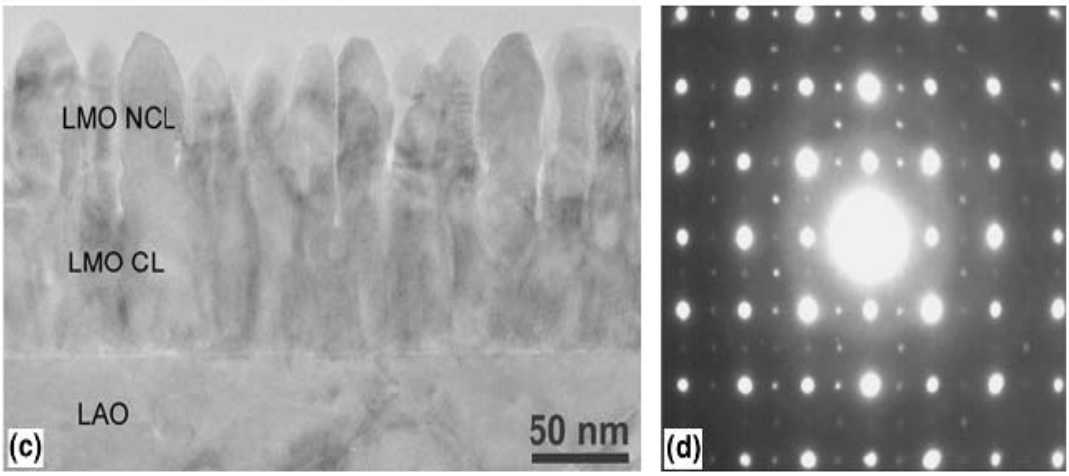

Figure 3.11 Cross-sectional TEM of (c) LMO/LAO deposited at 700 °C showing continuous layer (CL) and nano column layer (NCL) structures. (d) SAED pattern taken from the column layer in LMO film.

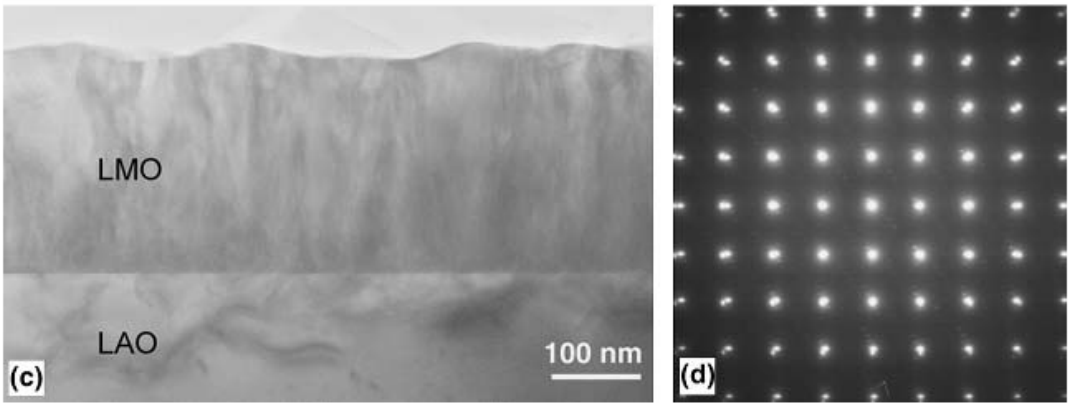

Figure 3.12 Cross-sectional TEM image and (d) SAED pattern of LMO/LAO deposited at 800 °C.

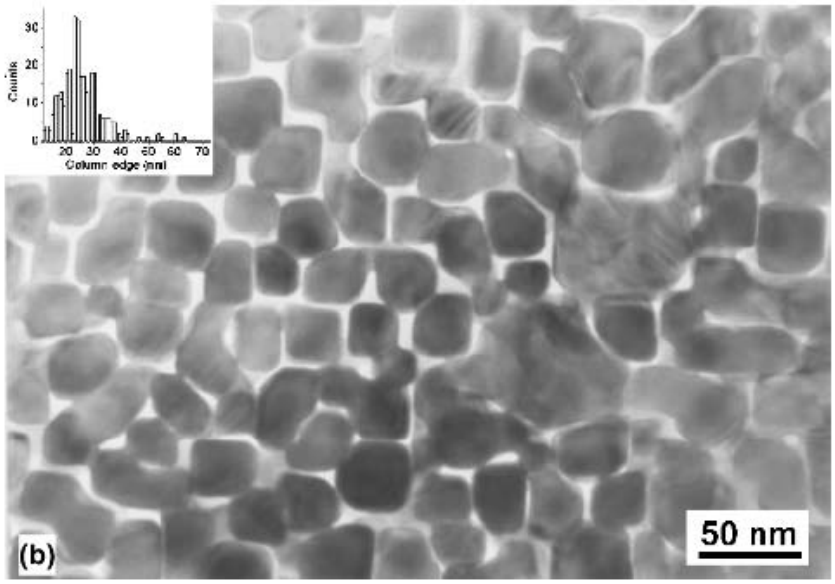

Figure 3.13 Plan-view TEM of (b) LMO thin film deposited at 700 °C.

3.4.5. Sputtering

Sputtering is a vacuum deposition process, which uses energetic ions to knock atoms or molecules out from a target that acts as one electrode and subsequently deposit them on a substrate acting as another electrode. Various sputtering techniques are used at present like DC sputtering, RF and pulse magnetron sputtering, reactive sputtering etc.; the fundamentals of the sputtering process are the same. Sputtering is driven by momentum exchange between the ions and atoms in the material, due to collisions. The principles of sputtering systems are shown as in Figures 3.14 and 3.15.

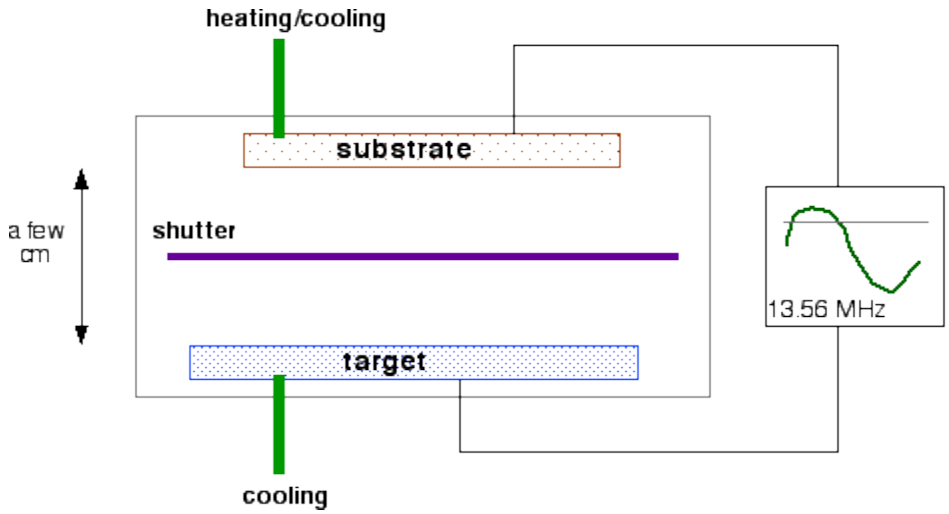

Figure 3.14 Schematic of a RF Sputtering System.

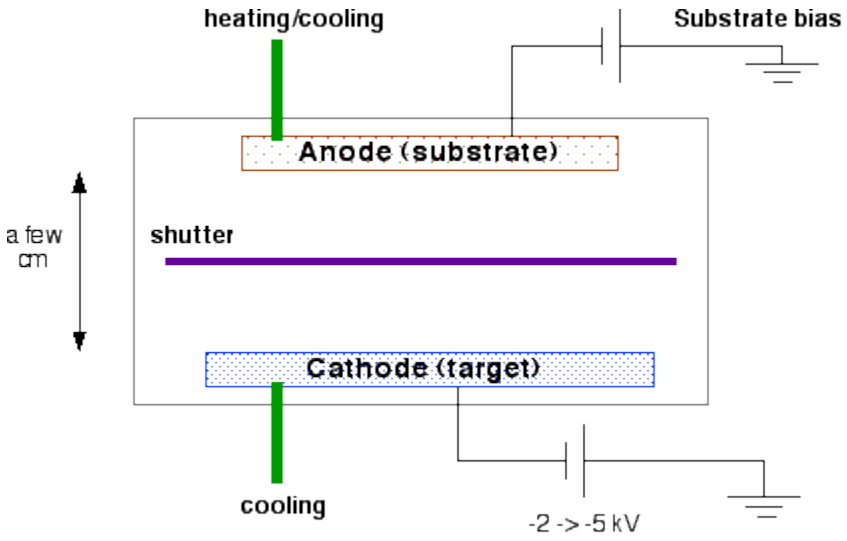

Figure 3.15 Schematic of a DC Sputtering System.

Target and substrate serve as electrodes and face each other in a chamber. The chamber is maintained under high vacuum. Then an inert gas, typically argon is introduced in the chamber with very low pressure that ranges from a few mTorr to 100 mTorr, as the medium to initiate and maintain the discharge. When an electric field of several kV is applied between cathode and anode, i.e., target and substrate, a glow discharge is initiated and maintained

between electrodes. Free electrons will be accelerated due to the electric field and it ionizes the argon gas by gaining high amount of energy. Argon ion Ar^+ will be attracted towards cathode and will hit the target, which will result in ejection of neutral atoms from target surface through momentum transfer. These atoms will pass through the discharge and will deposit on the substrate.

3.4.5.1 Physics of Sputtering

The target atoms will sputter; if only enough energy is transferred to overcome the forces bind them. Energy E_{th}, the threshold energy; the minimum energy is needed to unbind them. The typical value of this energy is ranging from 5 eV to 40 eV that depends upon the nature of incident ion and atomic and mass number of target atoms. Also the energy that binds the atoms to the surface should be taken into notice. This energy is denoted by U_s and is typically assumed to be the heat of sublimation having values between 2 eV and 5eV. Sputtering is the result of momentum transfer and the sputter yield S, which is the measure of sputtering efficiency, can be defined as,

S= (No. of sputtered atoms) / (Incident particle)

3.4.5.2 RF Sputtering

The RF sputtering system uses an RF power supply and a matching network. The power supply works at high frequency. The most common frequency is 13.56 MHz. RF sputtering essentially works because the target self-biases to negative potential. Once this happens, it behaves like a DC target which positive ion-bombardment sputters away atoms to subsequent deposition. For a small part of RF cycle, the cathode and anode are electrically reversible. This eliminates charge buildup on an insulating surface, by providing an equal number of ions, then electrons, then ions and then electrons. This allows insulators to be sputtered or metals to be sputtered in reactive environment,

Another advantage of RF system is that the oscillation of the fields in the plasma results in additional electron motion within the plasma results in enhancement in electron movement that

the probability of an ionizing collision is increased for a given secondary electron, and this result in increase of the plasma density.

3.4.5.3. Magnetron

A magnetron uses a static magnetic field configured at the cathode location. The magnetic field is located parallel to the cathode surface. Secondary electrons, which are emitted from cathode due to ion bombardment, are constrained by this magnetic field to move the direction perpendicular to both electric and magnetic field. This is known by ExB drift. This drift causes electrons to move parallel to the cathode surface and perpendicular to magnetic field. If the magnetic field set-up correctly, this drift can be arranged to close on itself, forming a current loop of drifting secondary electrons. These secondary electrons are essentially trapped in a region close to the cathode. Eventually they lose their kinetic energy due to collision with gas atoms and the net result is extremely dense plasma. Ions in this drift ring have a high probability of hitting the cathode.

3.5 Epitaxial and Polycrystalline Thin Films Growth

3.5.1 Epitaxy

Epitaxy is a very special process that refers to formation of single crystal on top of a single crystal substrate. Epitaxial growth is mainly falls in two main types; homoepitaxy and heteroepitaxy. Homoepitaxy is the process in which the material film grown is same as the substrate material e.g. epitaxial silicon deposited on silicon wafer which gives more defect free surface, purer than bare wafer and can be doped independently. Homoepitaxial films are mainly grown to improve the quality of base materials.

Heteroepitaxy is the process in which the film materials are different than that of substrate material. Optoelectronic and magneto electric devices, which contain compound semiconductor or magnetic thin films, are based on heteroepitaxial film structures.

The obvious difference between homoepitaxial and heteroepitaxial thin films is the lattice mismatch between film and substrate materials. In homoepitaxial thin films there is no lattice mismatch present as both film and substrate materials are same. In heteroepitaxial films there is a certain lattice mismatch present in substrate and film. This mismatch can be given by the formula

$$F = (a_s - a_f) / a_f \quad (3.7)$$

where, a_s is lattice parameter of unstrained substrate and a_f is lattice parameter of unstrained film material. If F>0 then the film is strained in tension otherwise it is strained in compression. The strain energy E that develops in strained films can be given as,

$$E = 2\mu_f \{(1+v) / (1-v)\} \varepsilon^2 t.A \quad (3.8)$$

where, μ_f is shear modulus of film, v is the Poisson's ratio, ε is the plain or lateral strain t is thickness and A is the surface area. The strain energy can be accommodated by straining both film and substrate, when the mismatch is small or relaxed by formation of dislocations, where mismatch is large.

3.5.2. Polycrystalline film

The microstructural characteristics of polycrystalline films control their properties, performance, and reliability in applications tiepin a wide variety of electronic, magnetic, photonic, chemical and micromechanical devices and systems. These films are used in interconnect devices in IC's, magnetic storage medias, catalytic elements, thermal teasing materials, piezoelectric materials in actuators and transducers Piezoelectric and ferroelectric thin polycrystalline films are used in surface acoustic wave transducers and in head of magnetic storage media.

3.5.3. Thin film growth

The process of growth of a material on a substrate as a thin film, on either epitaxial or polycrystalline form can be divided into six general steps as:

1. Nucleation
2. Coarsening
3. Coalescence
4. Grain Growth
5. Recrystallization
6. Thickening

Thin film formation on a substrate initiates through the nucleation of isolated crystals on a substrate surface. Nuclei grow into external phase and lateral direction in plane of interphase. Coalescence is the result of lateral growth. Coalescence leads to formation of grain boundaries. This defines the initial grain structure characteristics of film.

Nucleation and coalescence results in formation of film less than 10 nm; but for most of the applications further thickening of the films are required. Grain structure evolution during thickening, occurs in two fundamentally different ways. If the grain boundaries formed through impingement are immobile, the grain structure resulting from nucleation, growth and coalescences processes is retained as the base for the film. Usually, subsequent thickening occurs through epitaxial growth on these grains and columnar grain structure develops.

In polycrystalline films, the grain structures do not have the same crystallographic orientations. Very often, polycrystalline films have a crystallographic texture in which the crystals form are composed of specific crystallographic directions normal to the plane of the film. The grain orientation distribution evolves and can be controlled during film formation and processing.

CHAPTER 4

EXPERIMENTAL DESIGN AND PROCEDURE

The present work involved two parts. First, a study was conducted involving LMO thin film deposition on Si wafers using RF magnetron sputtering. The goal was to investigate the effect of processing parameters like deposition temperature, RF power, sputtering pressure on the quality of the LMO film. Based on the findings of the first part, LMO thin films were deposited on two additional substrates, i.e., MGO (MgO) and LAO ($LaAlO_3$) substrates to study misfit/interface effects on film quality. A study of the magnetic and surface properties was performed. All deposition was conducted using the home built hybrid CVD/PVD system. The details of the deposition system are given below.

4.1 Deposition of LMO Thin Films

4.1.1 PVD/CVD/Sputtering System

LMO thin films were deposited using home built vacuum deposition system combining magnetron sputtering and CVD in the Surface and Nano Engineering Laboratory (SaNEL). A schematic representation of the system is shown in Figure 4.1. The stainless steel chamber has a cylindrical shape, with 46.68 cm diameter and 49.93 cm in height. The system has two Magnetron guns (2” diameter) equipped with both, DC and RF biasing capabilities. The guns can hold targets of thicknesses 0.125”, 0.185” and 0.250”. The targets are shielded using a pneumatic shutter over the magnetron gun. The guns can be RF powered up to 300W using an AJA Seren RF generator and manual matching network. The substrate has rotation, both RF and DC biasing and heating up to 850° C capabilities. The substrate holder has a 10 cm end plate where the samples can be mounted. The substrate can be either RF or DC biased up to 50W and 1000V respectively. The maximum power that can be applied as substrate bias is 50W. Roughing is accomplished down

to <20 mTorr by a Trivac 30A mechanical pump and beyond that vacuum is achieved by an Ebara FS 8 series cryopump and compressor. The base pressure can reach 10^{-7} torr. Prior to deposition, the cryopump is roughed down to 20 mTorr for 45 mins using the mechanical pump. It is helpful in partial regeneration of the cryopump and also helps it to reach lower temperature. After that, the compressor is started to cool the cryoarrays down to 10 K. This helps in creating very clean vacuum inside the chamber during deposition. During the cryo cooling, the gate valve is closed to isolate it from the chamber.

During deposition, very precise pressure control is maintained using an automatic 8" gate valve (Kurt J. Lesker) in conjunction with a MKS 146C PID controller. Three different pressure gages have been installed in the system for different purposes. The thermocouple gage measures the roughing line pressure, whereas the baratron measures the chamber pressure during deposition and gives input to the gate valve for maintaining set point pressure. The ion gage measures the pressure, when the chamber is exposed to the cryopump for creating high vacuum. It operates only under a pressure below 10^{-4} mTorr. The flow of gases during deposition is controlled using Unit Instruments mass flow controllers and a read out box. During the deposition, the substrate was heated by using an AJA SHQ-15 substrate heater. The heater can heat the substrate up to 900^{o}C.

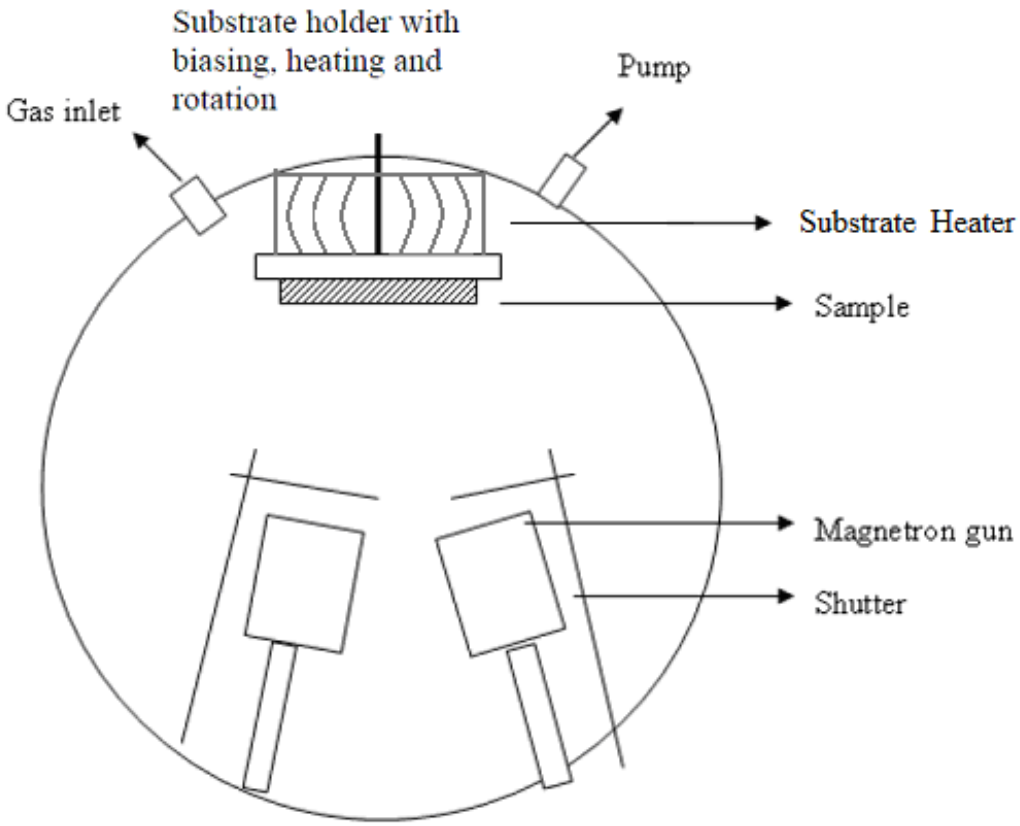

Figure 4.1 Schematic Representation of home made DC/RF Sputtering System.

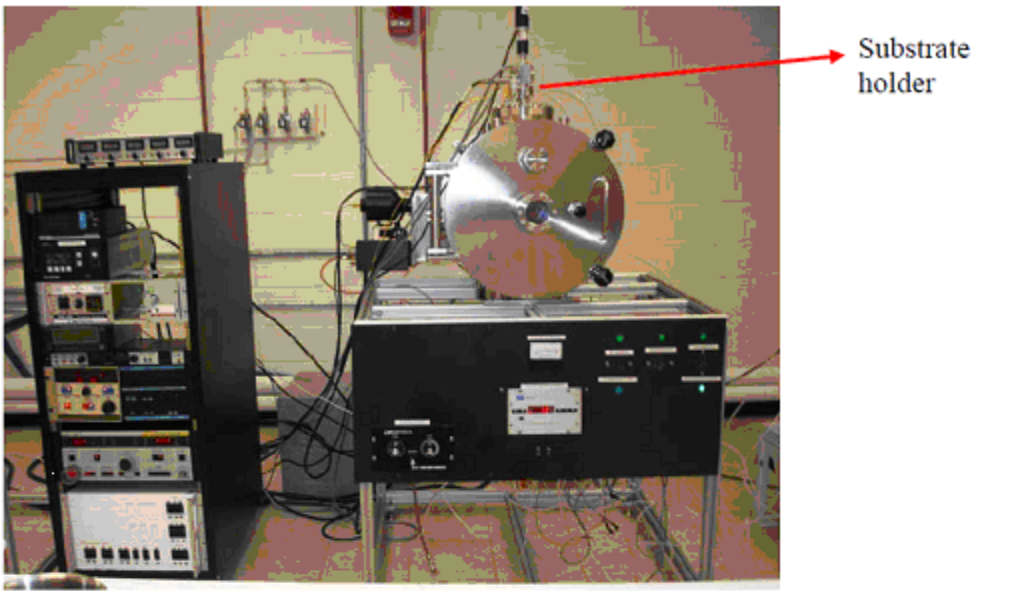

(a)

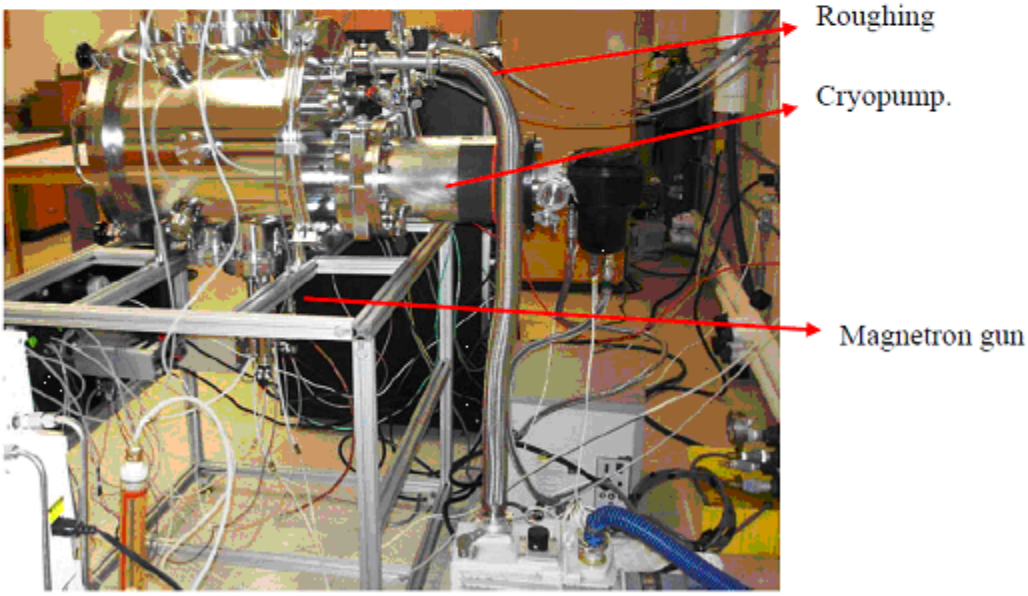

(b)

Figure 4.2 (a) Front view of the system (b) Side view of the system.

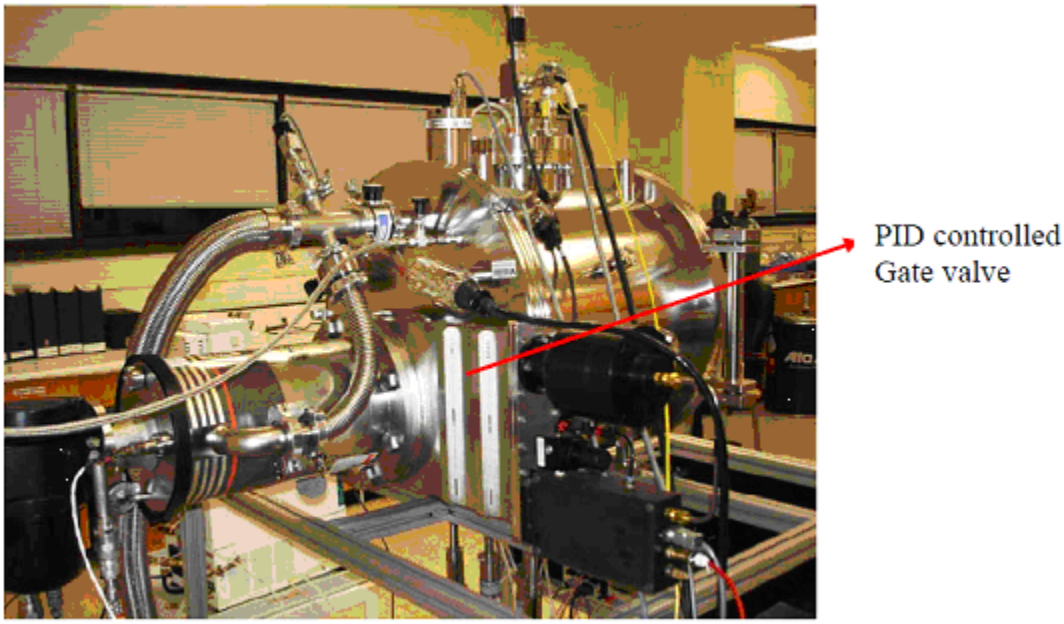

Figure 4.3 Side view of the sputtering system.

4.2 Deposition Procedure

4.2.1 LMO Deposition Parameters

Three substrates materials were used for LMO deposition, namely Si (100) p-type wafers, 2.5 x 2.5 x 0.5mm thickness, 1 side epitaxial polished MgO (100) substrates (provided by MTI crystals inc.) and 1.25 x 1.25 x 0.5mm thickness, 1 side epitaxial polished LAO (100) substrates, also provided by MTI crystals Inc . The silicon wafers were first cleaned in acetone and then dried with compressed air, prior to deposition. Two LMO films were deposited on surface layer etched silicon wafer. To remove the surface SiO_2 layer, the wafers were immersed in 51% HF for 20 seconds. The removal of dioxide layer was confirmed by running water on the wafer. Then, the wafers were immersed in de-ionized water and then dried with compressed air. The MgO and LAO substrates were vacuum stored and were used as received condition. The wafer was masked in two areas at the edges. These masked areas were later used for measuring the film thickness using step height analysis. The chamber was roughed down to 15 mTorr using the

mechanical pump and then exposed to the cryopump by opening the gate valve. The base pressure of the chamber was around $3x10^{-6}$ mTorr. The chamber was purged two to three times with Argon prior to any processing. The substrate was sputtered cleaned with Ar at a bias of 35 W for 10 min at a pressure of 20 mTorr. Sputter cleaning removes any surface contamination and contributes to good adhesion of the films. All the LMO thin films were deposited by RF biasing the target in Ar atmosphere and applying heat to the substrate. LMO was initially pre-sputtered on the shutter plate to establish good plasma as well as to check the plasma stability. Then the shutter was opened when good quality plasma was established. The sputtering was carried on power controlled mode. First, a series of deposition experiments were conducted to determine the processing conditions that results in quality films. All these depositions were conducted on Si wafers. The power was varied from 80W to 30W to study the effect of applied power on microstructure of films. The substrate temperature was also varied determine the temperature effects on microstructure of the films. The processing parameters are given in Table 4.1. Upon deposition, film thickness was measured using optical profilometry.

Table 4.1 Parameters for LMO Thin Films Deposition.

Sample	Substrate	Sputtering Pressure (mTorr)	Argon Flow (sccm)	Substrate Temperature (C)	RF Power (Watts)	Deposition Time (hrs.)
LMO-Si1	Silicon wafer	10	5	750	80	1
LMO-Si2	Silicon wafer	10	5	750	50	2
LMO-Si3	Silicon wafer	10	5	750	30	3
LMO-Si4	Silicon wafer	10	5	700	80	1
LMO-Si5	Silicon wafer	10	5	700	50	1
LMO-Si6	Silicon wafer	10	5	700	30	1
LMO-Si7	Silicon wafer	5	5	750	30	2
LMO-Si8	Silicon wafer	5	5	700	50	2
LMO-S1	Silicon wafer (etched)	10	5	750	30	3
LMO-S2	Silicon wafer (etched)	10	5	700	30	3
LMO-M1	MgO	10	5	750	30	4
LMO-L1	LaAlO3	10	5	750	30	4

4.3 Microstructural Characterization

4.3.1. X-Ray Diffraction (XRD)

The primary crystal structure and composition of deposited films was investigated by using x-ray diffraction technique. A Siemens D500 Diffractometer was used at the θ-2θ mode. The step size was 0.02 degrees and the dwell time was adjusted for 4 seconds. The accelerating

voltage was 40 kV and the accelerating current was 30mA. All the samples were investigated in the range of 20-65^0.

4.3.2. Energy Dispersive Spectroscopy (EDS)

Energy dispersive spectroscopy was used to conduct the compositional analysis of the LMO thin films. An Oxford Instrument EDS was used in conjunction with a JEOL JSM-6100 scanning electron microscope (SEM). The beam current was 0.2 mA and the accelerating voltage was 20kV.

4.3.3. High Resolution Transmission Electron Microscopy (HRTEM)

Plan view and cross section TEM samples were prepared for characterizing the microstructure and structure of the phases present. Cross section HRTEM samples were prepared using the following steps:

a. A small square section of the sample was cut using a diamond knife and was glued on the holder with thin film side facing the holder.

b. Two rectangular sections with size 3mm x 1mm were cut from the sample on an Isomet low speed saw.

c. Two small sections were removed from the holder and cleaned with acetone. The two sections, with thin film facing each other were glued with M Bond 610 adhesive. The sample was placed on the holder and heated for 20 minutes at 150^{o}C.

d. The sample was glued on the holder and grinded on an Ecomet variable speed grinder polisher at 120 rpm with three different diamond lapping paper size 6 μm, 3 μm and 0.1 μm respectively. The sample was ground till shiny surface was produced and all scratches were removed. The sample was removed from the holder and washed with acetone.

e. The thin film side of the sample was glued with the shiny side on copper grid with M Bond 610 adhesive. The sample was kept at the center of the copper grid and heated for 20 minutes at 150oC.

f. The sample was polished on the 600 grit polishing paper using distilled water. The sample was polished till its thickness reached 120 μm.

g. The sample was mounted on the Dimple grinder 656 and was aligned with the microscope. The sample was dimple ground with brass wheel using 3 micron diamond paste as a lubricant. The sample was further ground with stainless steel wheel using alumina paste as the lubricant and was then cleaned with acetone.

h. The sample was mounted on the precision ion milling system for ion milling. The pressure was set to 5 x 10^{-2} Torr with the stage rotation at 4 rpm. The sample was kept for ion milling till there was a small hole in the sample.

i. The sample was inspected under a Nikon Eclipse ME600 optical microscope. The sample was then ready for TEM analysis.

All TEM sample preparation and analysis was conducted by Mr. Yinsheng Fang from SaNEL, a part of his MS Thesis. Some of his results are presented here in the context of understanding LMO film deposition and properties.

4.3.4. Surface Properties

The selected samples were investigated for surface structure and electrical properties by using Agilent SPM 5500 atomic force microscope (AFM) with the facility of electrostatic force microscopy mode (EFM). The imaging was carried by non contact imaging mode.

In non contact mode, the tip of the cantilever does not contact the sample surface. The cantilever is instead oscillated at a frequency slightly above its resonance frequency, where the amplitude of oscillation is typically a few nanometers (<10 nm). The Van der Waals forces; which are strongest from 1 nm to 10 nm above the surface, acts to decrease the resonance frequency of the cantilever. This decrease in resonance frequency combined with the feedback loop system maintains a constant oscillation amplitude or frequency by adjusting the average tip-to-sample distance. Measuring the tip-to-sample distance at each (x, y) data point allows the scanning software to construct a topographic image of the sample surface.

In EFM mode, a conductive AFM tip interacts with the sample through long-range Coulomb forces. These interactions change the oscillation amplitude and phase of the AFM cantilever, which are detected to create EFM images. In an EFM image the phase, frequency, or amplitude of the cantilever oscillation is plotted at each in-plane (X, Y) coordinate. This phase, frequency, or amplitude is related to the gradient of the electric field between the tip and the sample. A voltage carrying AFM tip also enables electrical modification of materials on or beneath the surface

In the present study, Cr/Pt plated conductive AFM tips were used for the investigation which had resonance frequency of 190 KHz. The sample was electrically conducted and applied a voltage of 0.5-1.5 V. the sample was investigated for topography, EFM phase, X sensor of EFM phase, real time phase and real time amplitude.

4.3.5. Magnetic Properties

A vibrating sample microscope was used to investigate the magnetic properties of the samples exhibited at room temperature. A sample with size 3 mm x 3 mm was cut with a diamond knife and inserted into the Vibrating Sample Magnetometer (VSM). Hysteresis loop were acquired, for both in plane and out of plane magnetic field applied to the surface of the sample at 5000 Oe applied field.

The SQUID was used to determine the magnetic properties at very low temperature as well as to study the temperature effect on the magnetic properties. A sample with size 5 mm x 3 mm was cut with a diamond knife and inserted into the magnetometer. The hysteresis loop at temperature 10K and 100k was obtained at an applied field of 5000 Oe. Then the samples were run in the temperature range of 10K-300K to study the temperature effect on magnetic phase transition at a constant applied field of 200 Oe.

4.3.6. Annealing

Sputter deposited LMO films were found to be oxygen deficient. In order to improve crystallinity, small pieces of samples were annealed under an oxygen atmosphere at 800^0C for 4 hrs. MTI GSL 1300 tube furnace was utilized for annealing with oxygen constantly flowing from one side. All samples were annealed in one batch by placing them in the heating zone of the furnace. The heating cycle was 4 hours of which the temperature increased from room temperature to 200^0 C in within the hour at 3^0/minute. Then the temperature was increased to 800^0C next hour at the rate of 10^0/min. The temperature was kept constant at 800^0C for next one hour and at last the temperature was reduced to room temperature at 13^0/min. The annealed samples were also tested by XRD and TEM to study the effect of annealing.

CHAPTER 5

RESULTS AND DISCUSSIONS

5.1 Effect of Processing Parameters on Thickness and Deposition Rate of LMO Films

Magnetron sputtering in the RF mode has been used in the past to develop perovskite-type oxide films. Most of the previous studies deal with doped LMO films. For example, strontium, cesium and calcium doped LMO thin films have been deposited by Park and coworkers[29], Nakano and coworkers[31] and Gao and coworkers[32], respectively. In most of these previous studies, the as-deposited film was either amorphous-like or with very limited crystallinity. A post deposition annealing treatment was given to the films to promote crystalline epitaxial films. The range of the processing conditions used in the present study was selected by considering these previous reports [29,31,32].

A series of experiments were conducted to determine effective deposition parameters for producing quality LMO films. The initial study was performed on Si wafers to obtain such processing conditions and based on these findings, depositions followed on MgO and $LaAlO_3$ substrates. The processing parameters along with the deposition rate are presented in Table 5.1.

Comparing films LMO-Si 1 and LMO-Si 4 (deposited at different temperature), it can be seen that they merely the same deposition rate. Indeed, substrate temperature is expected to affect processes taking place on the film surface and not on the arrival rate of depositing specie.

Films LMO-Si 1, LMO-Si 2 and LMO-Si 3 were deposited to study the effect of applied RF power. The results show that the deposition rate increases by increasing RF power. A higher power provides higher energy to the Ar^+ that in turn increases the sputtering yield from the target.

Table 5.1 also shows that a very low deposition rate was obtained at 30 W of applied RF power and 10 mTorr pressure. Low deposition rates are desirable since they allow atoms to assume equilibrium positions in the LMO structure.

In film LMO-S 1 the inherent SiO_2 surface layer was removed. This deposition was carried out to evaluate possible effects of the presence (or absence) of the oxide amorphous layer. It can be seen from Table 5.1 that there is no considerable difference in the deposition rate between films on substrates with and without the oxide layer.

Table 5.1 Processing Conditions and Deposition Rates for LMO Thin Films

.

Sample Code	RF Power (W)	Substrate Temp. (^{0}C)	Deposition Time (h)	Substrate/HF Cleaning	Thickness (nm)	Deposition Rate (nm/sec)
LMO-Si1	80	750	1	Si/No	63	0.018
LMO-Si2	50	750	2	Si/No	57	0.008
LMO-Si3	30	750	3	Si/No	54	0.005
LMO-Si4	80	700	1	Si/No	61	0.017
LMO-Si5	50	700	1	Si/No	42	0.013
LMO-Si6	30	700	1	Si/No	22	0.006
LMO-S1	30	750	3	Si/Yes	58	0.0055
LMO-M1	30	750	4	MgO	72	0.005
LMO-L1	30	750	4	LAO	68	0.0047

It is interesting to note that all films deposited at low power (30 W) exhibited similar deposition rates regardless of the substrate type. Also, the deposition rate for all films was found to be in the range of 0.005-0.02 nm/sec. All depositions were carried out at 10 mTorr pressure and 5 sccm Ar flow rate. This rate of deposition is much lower than that reported by Malavasi and coworkers[33], which was 0.043 nm/sec. The reason behind the lower deposition rate in the present study is attributed to the greater target-substrate distance (15 cm as opposed to 5-10 cm) and

lower applied power (30 opposed to 145 W). The effects of the processing parameters on the microstructure of the film are discussed below.

5.2 Characterization of $LaMnO_3$ thin films

5.2.1. EDS Analysis

Selected films were analyzed for elemental stoichiometry using EDS in conjunction with SEM. Since the excitation volume is expected to be much larger than the film thickness, only the La:Mn ratio was considered to provide valuable information. Oxygen was involved in all these substrates thus, O content of the film is difficult to obtain. Table 5.2 presents the EDS analysis results. The La:Mn ratio was found to be near 1:1 in all the EDS analyzed films suggesting that the necessary stoichiometry in terms of La and Mn is maintained in the film.

Table 5.2 Composition Analysis of $LaMnO_3$ Thin Films

Film	Thickness (nm)	EDS Analysis, at. %		
		La	Mn	other
LMO-Si-2	57	1.39	1.36	74.13 Si 23.13 O
LMO-Si 3	54	1.44	1.43	72.26 Si 24.88 O
LMO-Si 4	61	1.49	1.43	74.20 Si 22.88 O
LMO-M 1	72	0.66	0.64	42.83 Mg 55.87 O

5.2.2 Effect of Processing Parameters on Film Microstructure

5.2.2.1 Effect of Substrate Temperature

Films LMO-Si1 and LMO-Si4 were deposited using the same conditions except the substrate temperature. Film LMO-Si1 was deposited at 750^{o}C and LMO-Si4 700^{o}C to access the effect of the substrate temperature. Figure 5.1 presents the XRD from these films in the as-

deposited condition. It is clear from the diffraction patterns that LMO-Si4 deposited at lower temperature shows a very broad peak suggesting a near amorphous (low degree of crystallinity) structure. On the contrary, the film deposited at 750^{o}C showed well developed diffraction peaks corresponding to a polycrystalline structure with a lattice parameter of 3.95 Å. Diffraction peak analysis of film LMO-Si1 shows that the grains were oriented in the (*l* 0 0) and (011) directions. The amorphous-like microstructure produced at 700^{o}C is supposed to be the result of the phase transition in LMO occurring at 735^{o}C as reported by Attaluri and coworkers[34]. Below 735^{o}C LMO remains amorphous and needs to be heated up above this temperature to crystallize. The present results are consistent with these previous findings. Cross-section TEM results of film LMO-Si 3 (also deposited at 750^{o}C) and 4 (performed by Mr. Fang) also confirm the amorphous and crystalline nature of the films, respectively, as shown in Figure 5.2. The TEM micrograph of film LMO-Si3 shows a polycrystalline structure with well developed columns along the entire film thickness. On the other hand, film LMO-Si4 shows an amorphous structure.

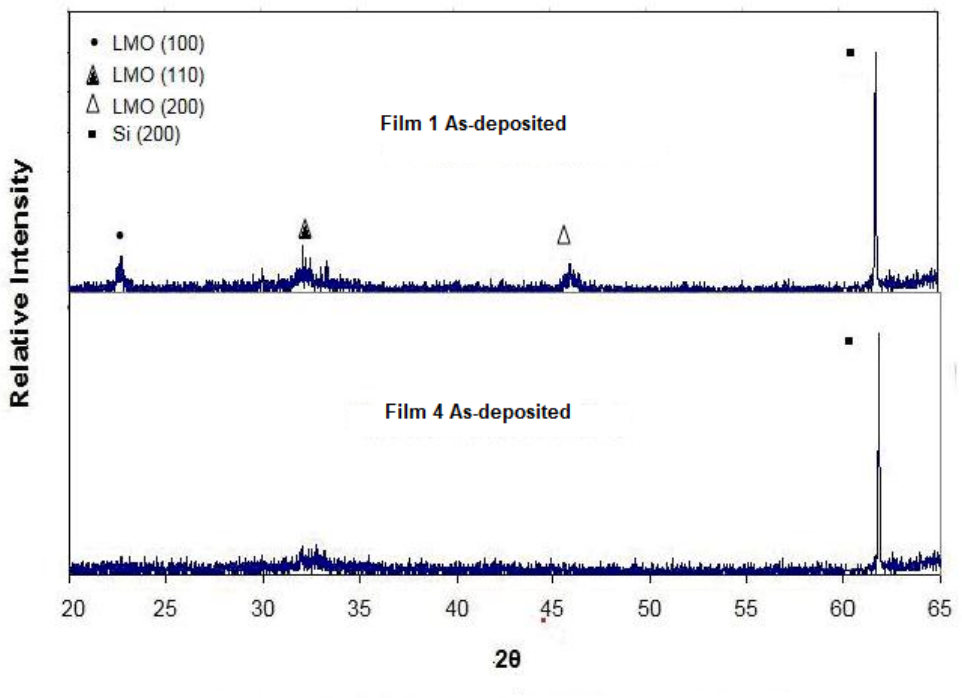

Figure 5.1 XRD patterns from LMO films deposited at 750^{o}C (Film 1) and 700^{o}C (film 4).

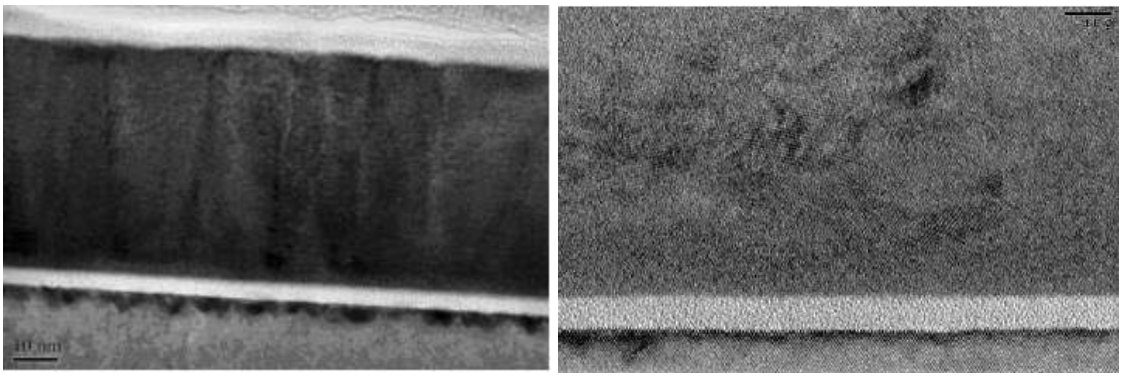

(a) (b)

Figure 5.2 Cross section TEM micrographs of LMO-Si (a) film 3, and (b) film 4.

5.2.2.2 Effect of RF power

Depositions were carried out to assess the effect of RF power. Films LMO-Si 1, LMO-Si 2 and LMO-Si 3 were deposited under the same conditions while the RF power varied from 80W, 50W and 30W, respectively. The XRD patterns taken from these films in the as-deposited condition are shown in Figure 5.3. The results show that the relative intensity of (100), (011) and (200) LMO peaks increases with decrease in applied power. Suh and coworkers[35] suggested that at lower deposition rate, adatoms are allowed sufficient time to migrate to the positions of local free energy minimum, resulting in higher crystallinity. The present XRD results are in agreement with this suggestion and show that the crystallinity of the deposited films increases with the decrease in RF power for the range tested.

Cross section and plan view TEM micrographs for films LMO-Si2 and 3 are shown in Figures 5.4 and 5.5, respectively. Better crystallinity with decrease in power can be confirmed from these micrographs. The plan-view TEM micrographs in Figures 5.5 (a) and (b) show the increase in the average grain size from 30 nm to 50 nm with decrease in power from 50W to 30W. Malavasi and coworkers[33] reported that the grain size in Na doped LMO films deposited at 145W RF power was around 20 nm. The present results are in agreement with the latter report and show that the grain size can further decrease (<30 nm) with increase in power beyond 50W.

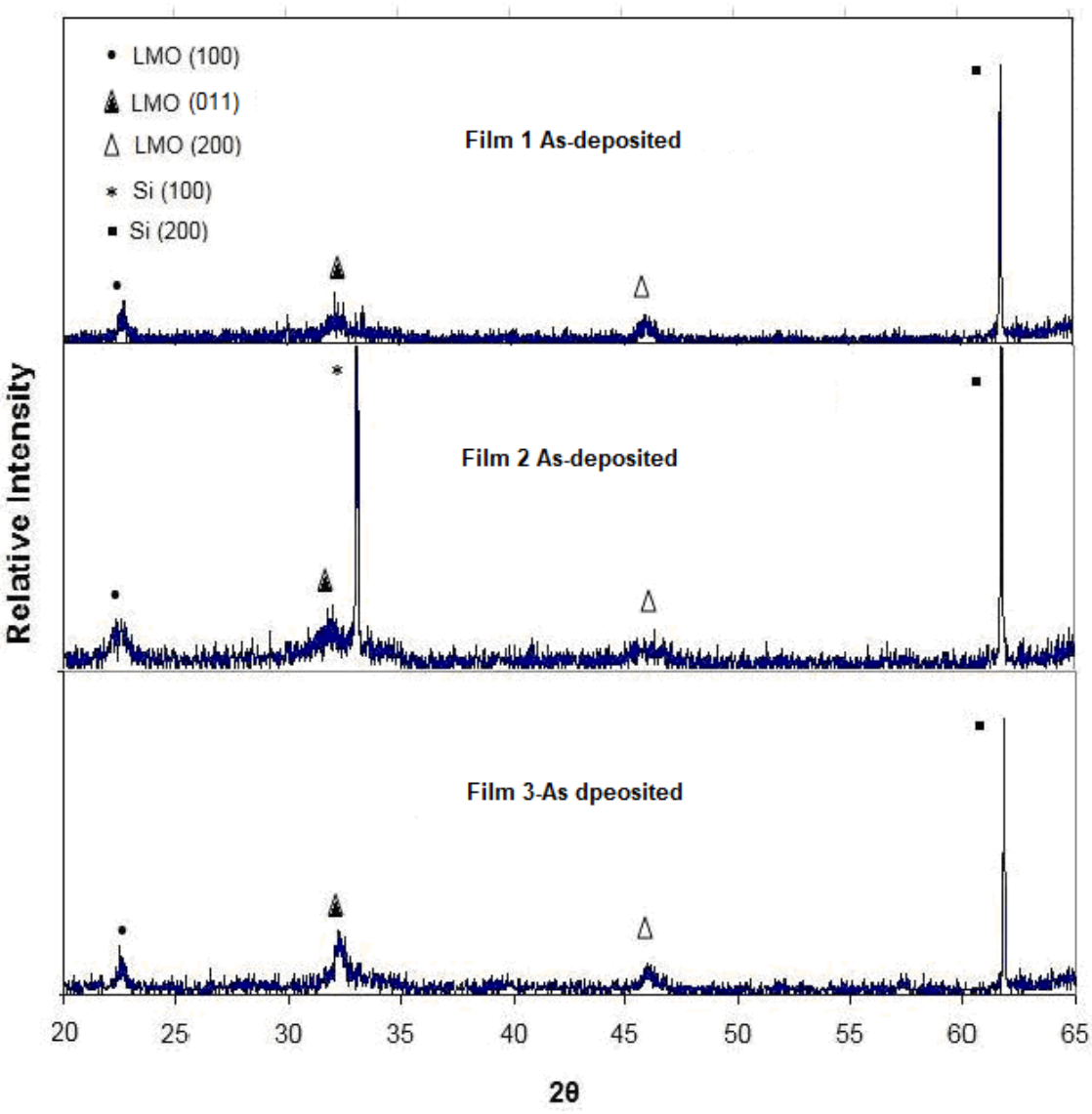

Figure 5.3 XRD patterns of film LMO-Si 1, LMO-Si 2 and LMO-Si 3 deposited at different RF power.

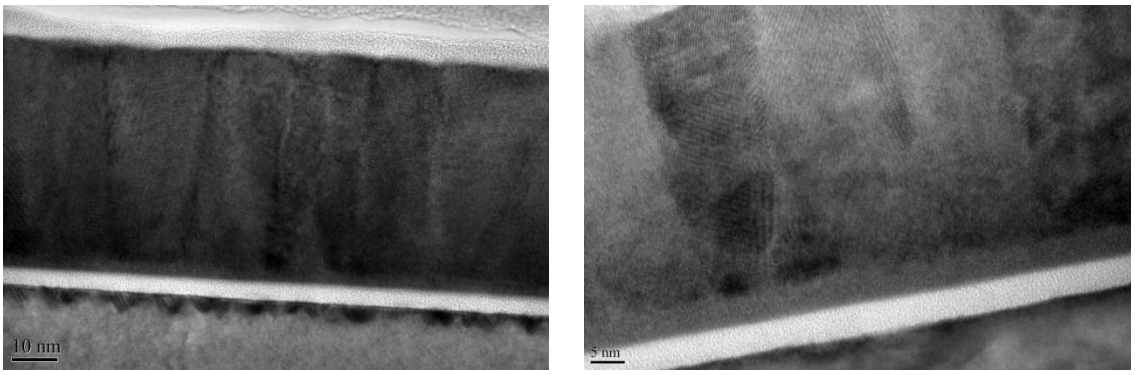

(a) (b)

Figure 5.4 Cross section TEM micrograph of (a) film 2 and (b) film 3.

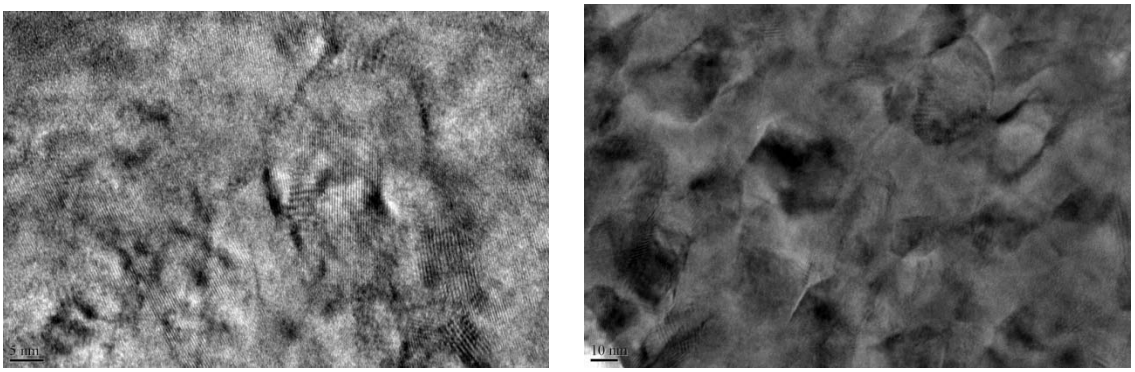

(a) (b)

Figure 5.5 Plan-view TEM micrograph of (a) film 2 and (b) film 3.

5.2.2.3 Effect of Silicon Etching

Film LMO-S 1 was deposited by using the same conditions for film LMO-Si 3. The only difference was the removal of the top oxide layer of the silicon wafer. The silicon wafer for film LMO-S 1 was etched in 51% concentrated HF for 20 seconds and then rinsed in DI water. Table 5.1 shows that there was no difference in the deposition rate between these two films. Furthermore, the XRD patterns from these films presented in Figure 5.6 show polycrystalline films for both cases. However, better crystallinity was obtained for the film LMO- S 1.

After the removal of the native amorphous oxide layer, the LMO film is expected to nucleate and grow on the crystalline silicon structure. The results suggest that this crystalline

silicon surface promotes LMO nucleation and growth. However, the deposition rate is determined mostly by the sputtering yield of the target that is directly related to the power applied.

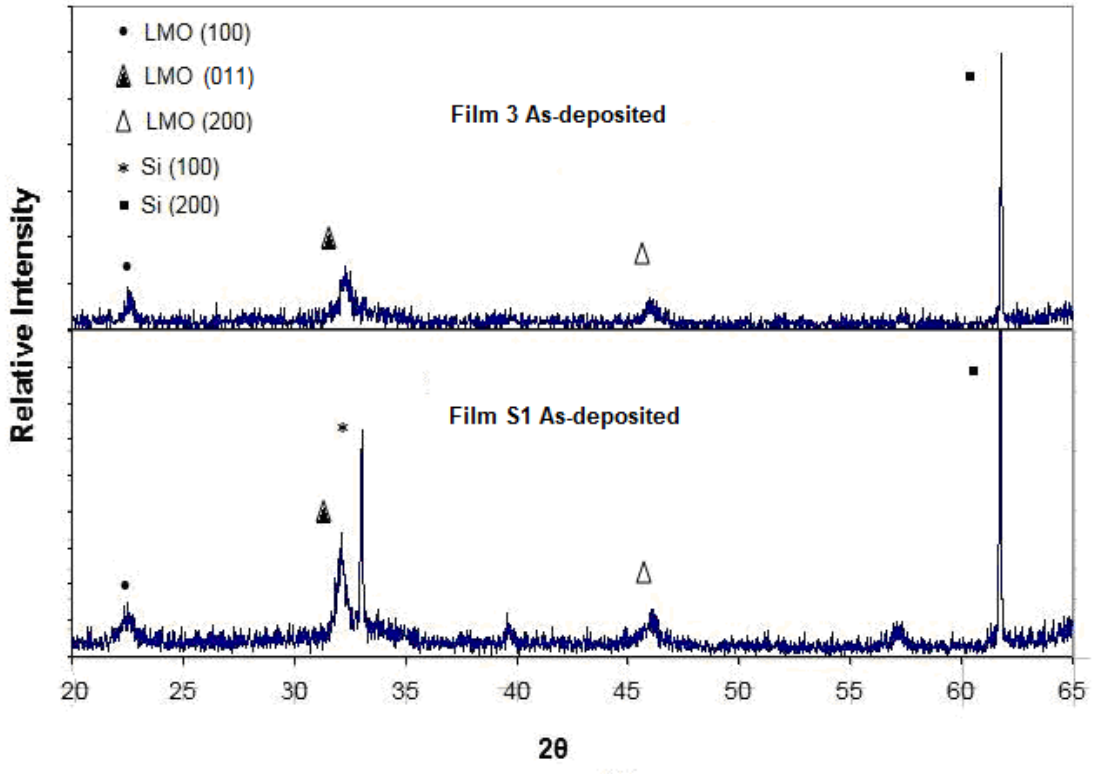

Figure 5.6 XRD patterns from LMO-Si 3 and LMO-S 1 films deposited on Si and etched Si wafers.

5.2.2.4 Effect of Substrate on Film Microstructure

Based on the findings from the previous series of experiments, the processing parameters of film LMO-Si3 were selected for deposition on two additional substrate materials, MGO and LAO. Films LMO-M1 and LMO-L1 were deposited on MgO and $LaAlO_3$ substrates respectively, using the same parameters as those for film LMO-Si3 LMO-S1 (etched wafer). The XRD patterns from these four films are shown in Figure 5.7. The lattice constants of Si, MgO and $LaAlO_3$ are 5.43 Å, 4.21 Å and 3.80 Å, respectively. The lattice constant of the as-deposited LMO films calculated from the XRD patterns in the present work was a =3.95 Å. Hence, the lattice

misfit of the LMO film with Si, MGO and LAO is -27.2%, -7.945 and +2.3%, respectively. A negative sign indicates compressive stresses. The XRD results show that the film developed on Si exhibited a polycrystalline structure having dominant (100), (011) and (200) peaks. On the contrary, the films deposited on (100) MGO and (100) LAO substrates show only (*l00*) peaks indicating formation of epitaxial films. These results are consistent with XRD results for LSMO and LCMO thin films reported by Park and coworkers[30].

The MGO and LAO substrates were single crystal and epitaxially polished. Also, compared to Si, the lattice misfit between these two substrates and LMO film is relatively small. Hence, these substrates provided a more favorable atomic surface structure in terms of lattice misfit to nucleate and grow an epitaxial film. Lower lattice misfit promotes a one-to-one atomic correspondence across the interface resulting in film epitaxy. The present results show that the misfit strain for the Si substrate was too large to allow deposition of an epitaxial film. The LMO film grown on the Si substrates show a preferred <011> growth direction that is perpendicular to the <100> substrate orientation.

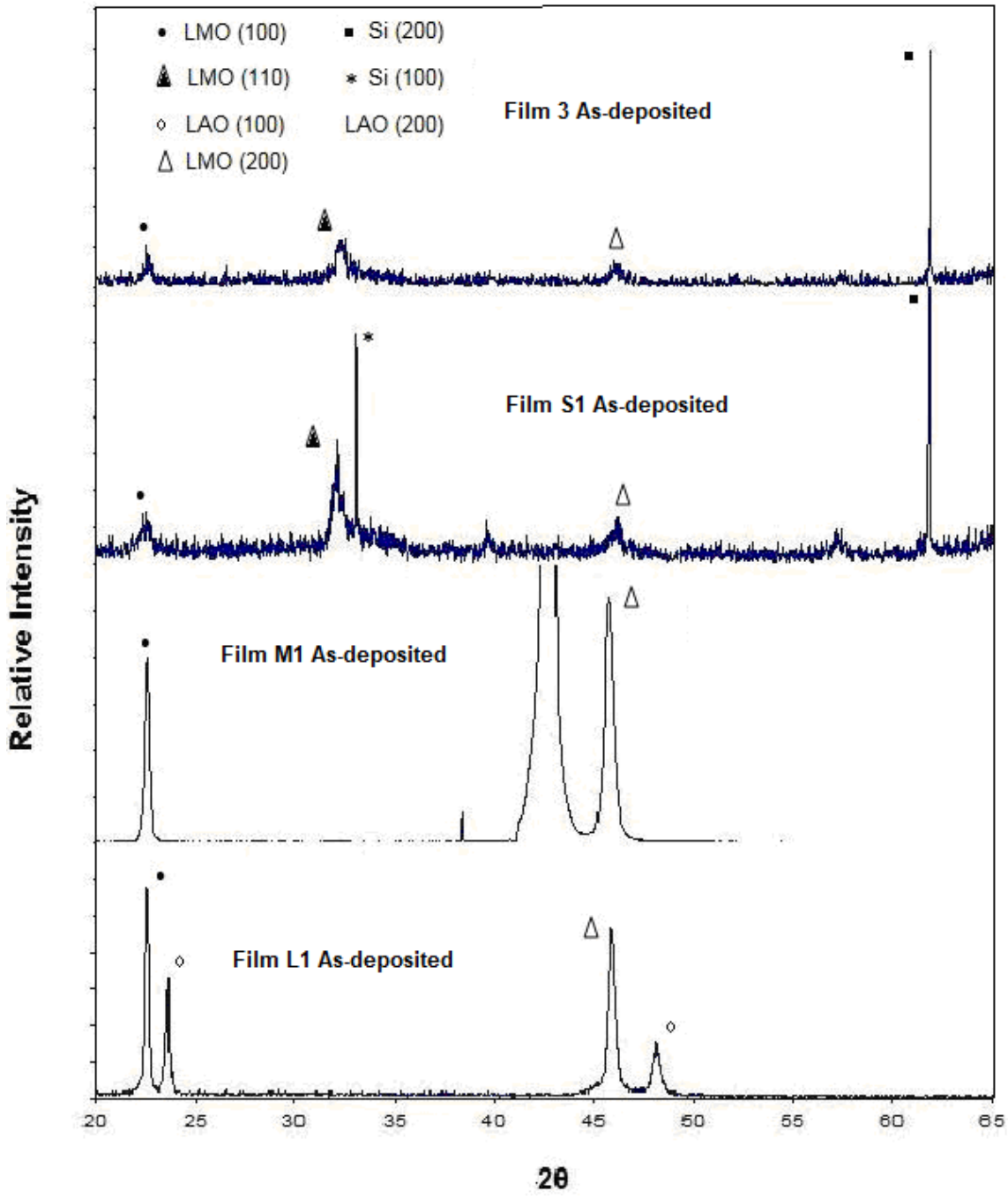

Figure 5.7 XRD patterns for LMO thin films deposited on different substrates.

5.2.2.5 Effect of Annealing

The lattice parameter calculated for the deposited LMO films was a = 3.95 Å, which shows a small deviation from the ideal lattice parameter of $LaMnO_3$, a = 3.87 Å. The somewhat larger lattice constant of the as-deposited films is due to oxygen deficiency in the LMO unit cell. This is typical for most oxides films deposited by sputtering due to preferential sputtering of oxygen that can deviate from the direction of deposition. To obtain the desired oxygen stoichiometry and improve film crystallinity, annealing experiments of selected films were performed as described in Chapter 4. The comparison of XRD patterns of as-deposited and annealed LMO-Si 3 film is shown in Figure 5.8. It is evident that after annealing, the intensities of the diffraction peaks are significantly increased compared to those of the as-deposited film. It is also noted that the peaks of the annealed film are shifted to larger 2θ values compared to the as-deposited film. The calculated lattice parameter of the annealed film was 3.87 Å. The results show that annealing at 800^0C for 4 hrs fills the vacant the oxygen lattice sites observed in the as-deposited film.

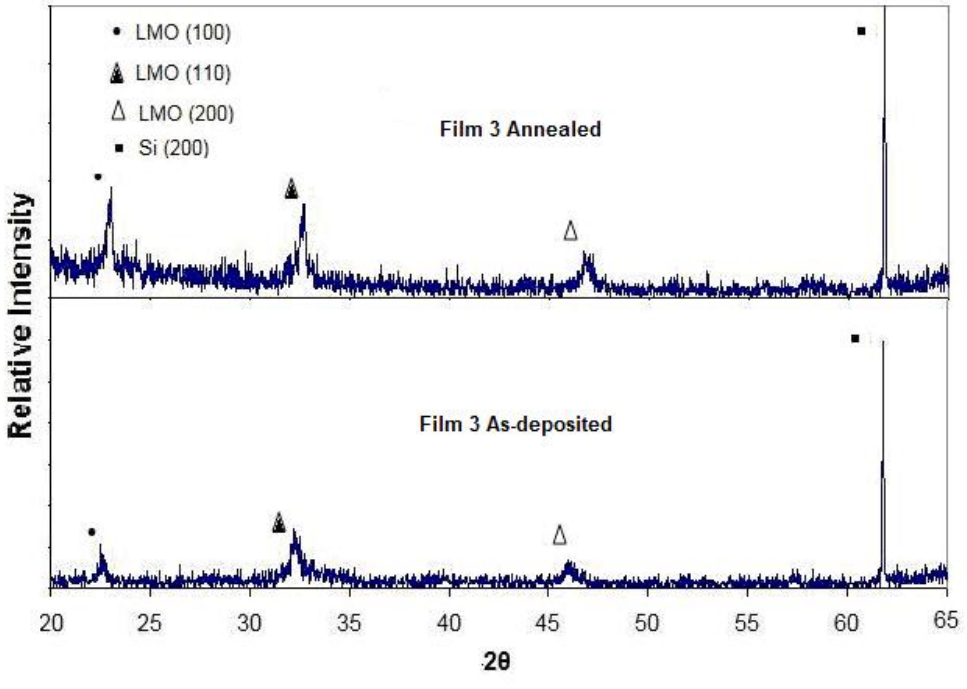

Figure 5.8 XRD patterns for film LMO-Si3 in the as-deposited and annealed condition.

5.2.3 Transmission Electron Microscopy[1]

TEM samples were prepared from selected films as discussed in Chapter 4. The TEM cross sections of LMO films on Si, MGO and LAO are as shown in Figures 5.9, 5.10, 5.11 and 5.12. The high-resolution cross section TEM image of LMO-Si film shows a polycrystalline grain structure for the majority of the film. A small amorphous layer of LMO can also be observed at the interface with the substrate. More than likely, the formation of this amorphous layer is resulting from the amorphous SiO_2 layer on top of the Si wafer. The SAED pattern (in set in Figure 5.9) consists of diffraction rings, clearly showing a polycrystalline structure for this film that is consistent with the XRD results. The first three rings correspond to the (100), (011) and (200) LMO reflections.

The HRTEM cross section micrograph of LMO-MgO film, Figure 5.10, shows a sharp interface and epitaxial (100) columns along the entire film thickness. The SAED pattern (in set in Figure 5.10) taken from the substrate/film interface clearly shows a single crystal film with high epitaxial quality. The HRTEM of the interface, Figure 5.11, clearly shows the epitaxial (100) growth of the LMO film on the (100) MGO substrate. Again, the TEM results are in agreement with the XRD findings.

The HRTEM cross-section micrograph of LMO-LAO, Figure 5.12, also shows a sharp interface and an epitaxial film growth on the LAO substrate in agreement with the XRD pattern. The structure of the top layer of the film is not well defined. This may be a result of specimen preparation and cannot be prejudged from X-Ray diffraction pattern.

[1] This part was performed by Mr. Yinsheng Fang and some of his results are included, which are complementary to the present work.

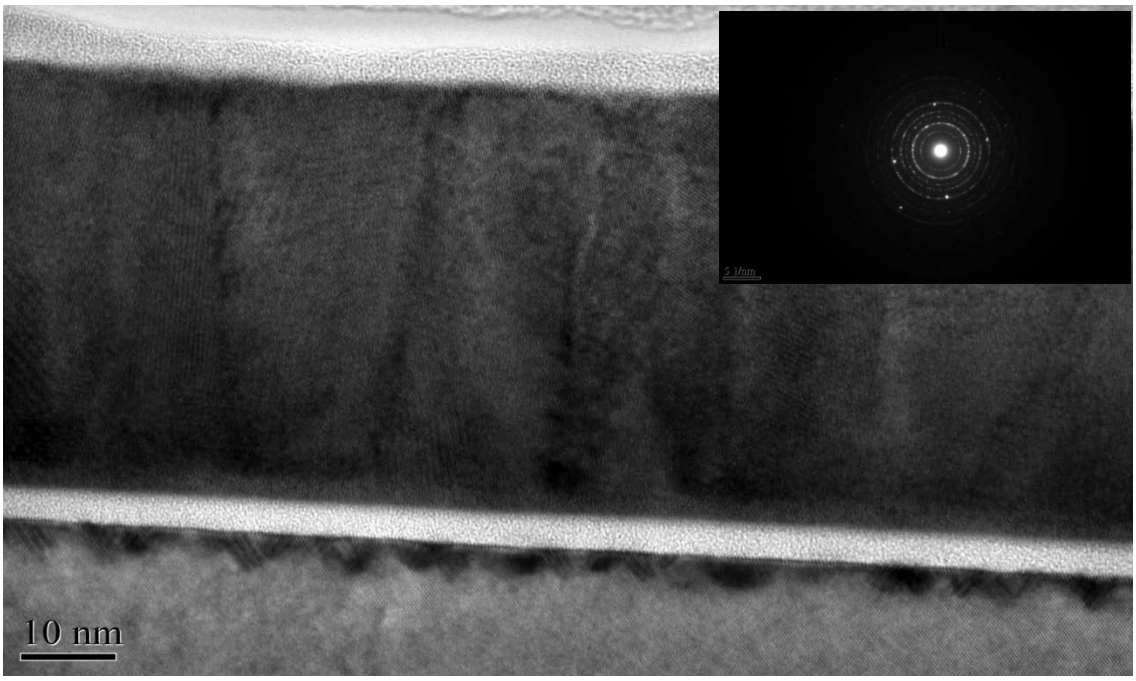

Figure 5.9 Cross section HRTEM and SAED pattern of LMO-Si 3 film.

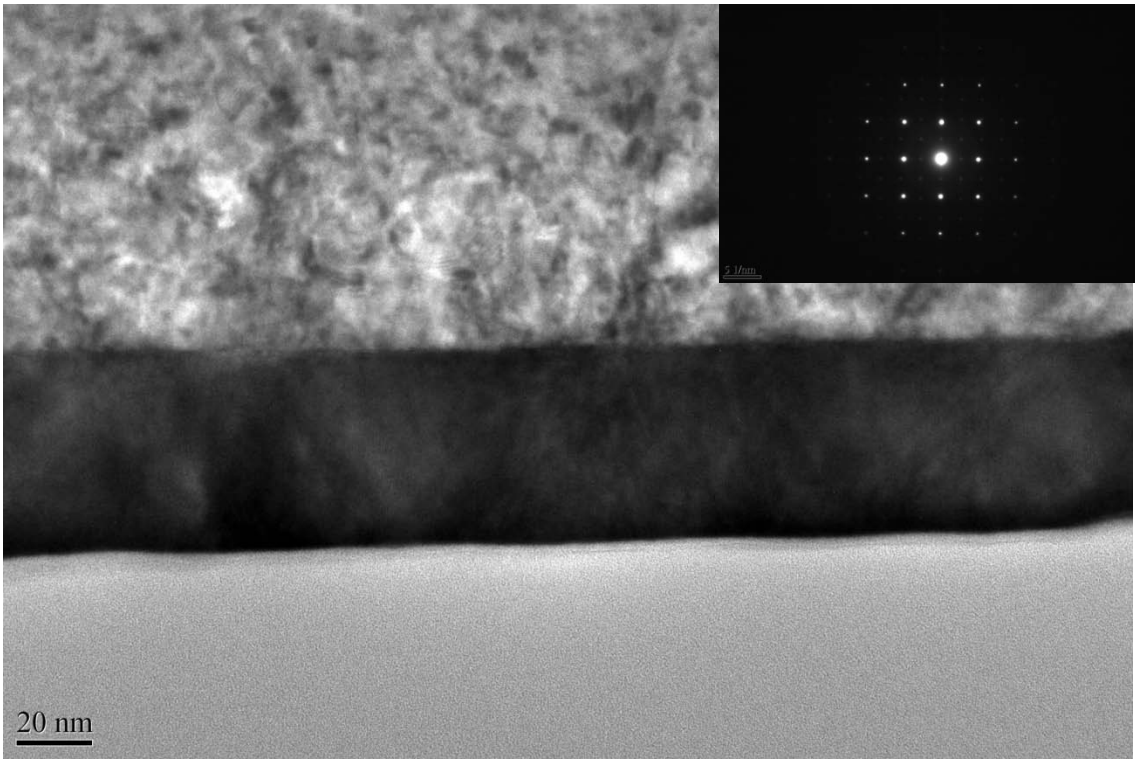

Figure 5.10 Cross-section HRTEM and SAED pattern of LMO-MgO film.

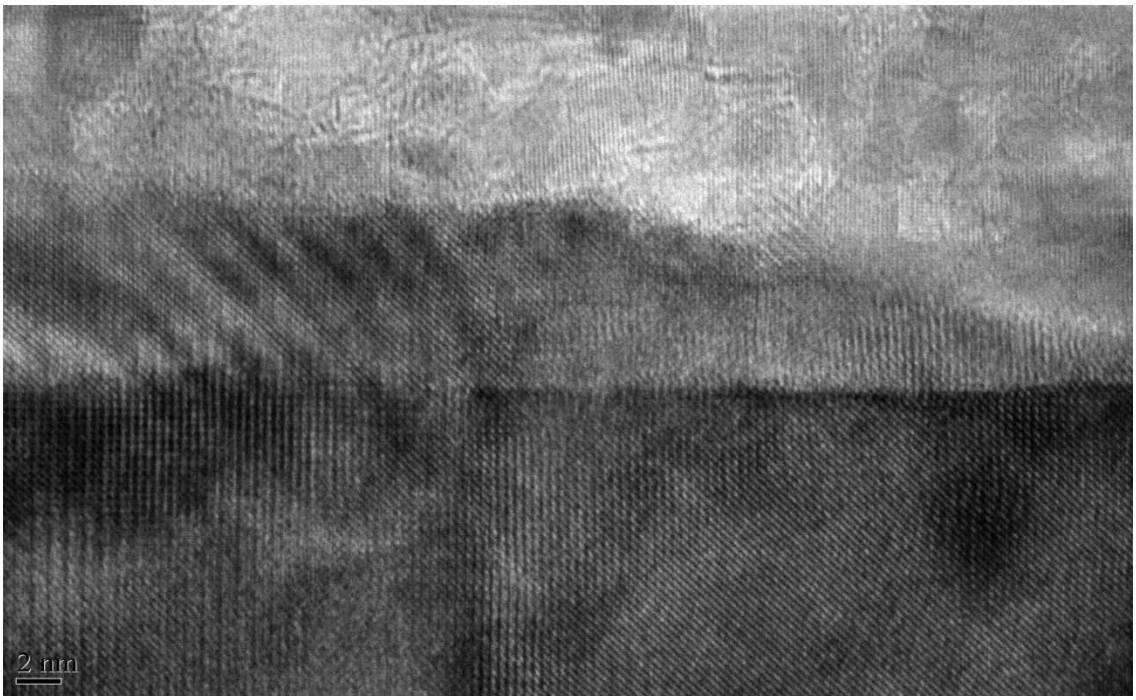

Figure 5.11 HRTEM micrograph of the interface of LMO-MgO film.

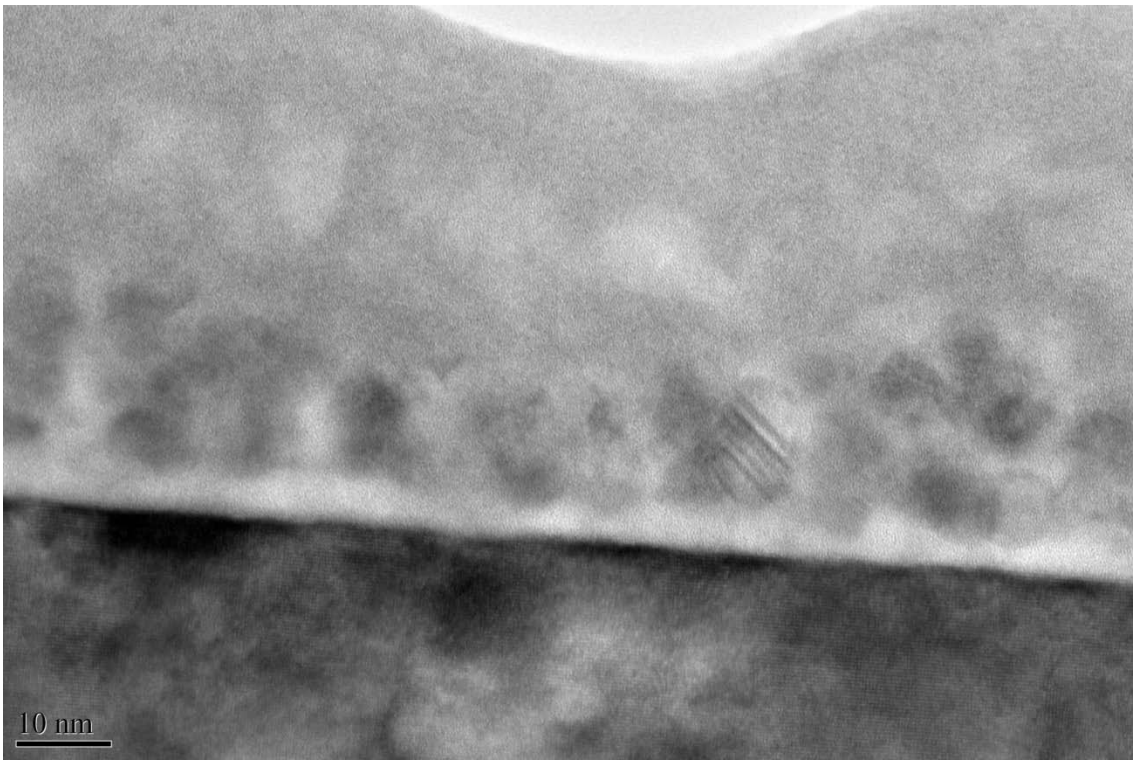

Figure 5.12 HRTEM cross section micrograph of LMO-LAO film.

5.2.4 Surface Properties

The nature of the surface of a thin film can play an important part in its magnetic and electrical properties. Especially, the surface of piezoelectric thin film plays a critical role in the performance of piezoelectric devices. Surface roughness is an important parameter for designing acoustic wave devices since a surface with high roughness will introduce defects between the film surface and the top electrode, and will introduce acoustic losses, as reported by Cibert and coworkers[37] and Wasa and coworkers[38]. Chen and coworkers[39] observed the electric pulse induced resistance-change effect at the nanoscale on $La_{1-x}Sr_xMnO_3$ thin films by current measurement AFM.

Hence, in this study, surface morphology and electrical response was investigated by using AFM with electrostatic force measurement. The surface of LMO-MGO film was flat and homogeneously covered with a number of crystal flakes, Figure 5.13. The average surface roughness was found to be around 2 nm. The roughness for LNMO films reported by Malavasi and coworkers[33] was 0.7 nm. The increase seen in the roughness of LMO-MgO film; compared to that reported by Malavasi and coworkers[33], was the result of the deposited crystal flakes of LMO on surface.

The surface of the LMO-Si film, Figure 5.14, shows a submicron grain structure. The EFM phase image for both LMO-MGO and LMO-Si films are shown in Figures 5.13 (b) and 5.14(b), respectively. Neither EFM image shows an electrical phase change except a deflection of the tip from the flakes on the surface. The electrical resistivity changes near the Curie temperature for perovskite manganites; this explains the unchanged EFM phase, as the temperature of phase change in LMO is 140K.

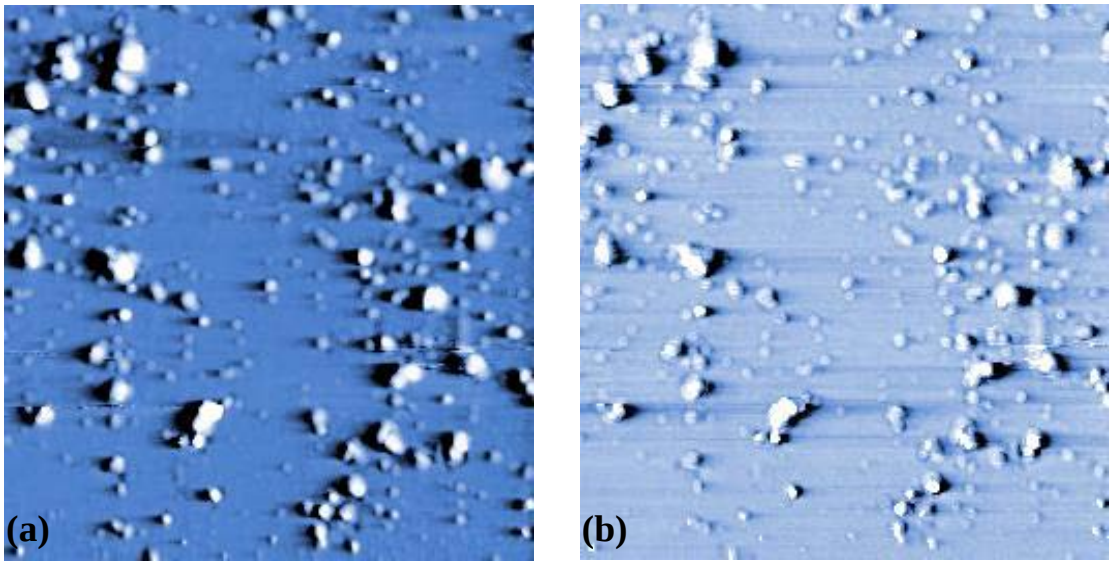

Figure 5.13 (a) Topography and (b) EFM image of LMO-MgO film with surface cross section of 20 μm x 20 μm.

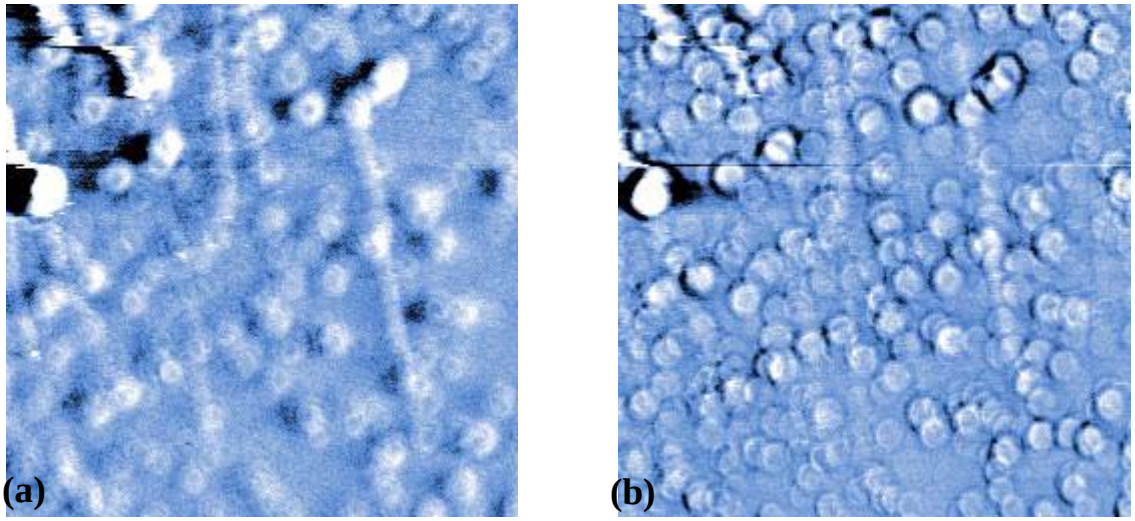

Figure 5.14 Topography (a) and (b) EFM image of LMO-Si with surface cross section of 20 μm x 20 μm.

5.2.5 Magnetic Properties

Films LMO-S1, LMO-M1 and LMO-L1 were selected for magnetic property measurement. The samples were tested on VSM at room temperature under -2000 to 2000 Oe applied field

range. All three films showed a paramagnetic nature with very little magnetic moment. A typical hysteresis loop is shown in Figure 5.15.

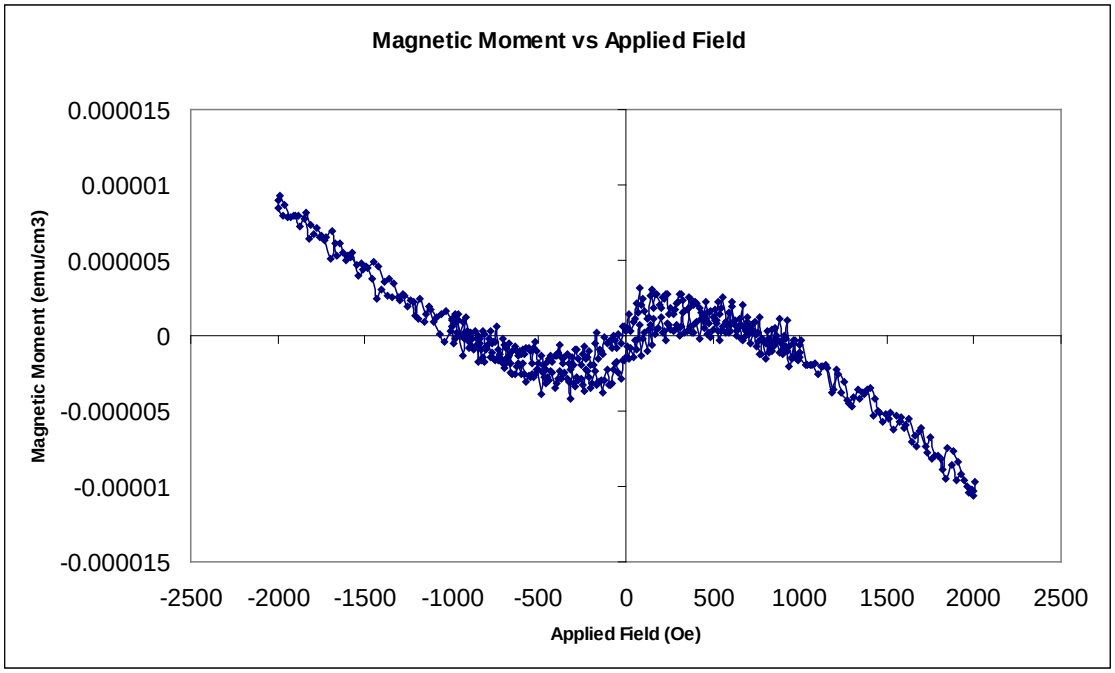

Figure 5.15 Typical hysteresis loop obtained from a LMO film at room temperature.

The magnetic phase transition temperature of bulk LMO is around 140K[35]. Hence, to investigate the magnetic properties of LMO, the selected films were studied by SQUID in the temperature range of 10 - 300K. The hysteresis loops were obtained at 10K and 100K for each film. The results are shown in Figures 5.16 and 5.17.

Magnetic moment is directly proportional to the magnetic susceptibility. The relationship between magnetic susceptibility and temperature can be given by

$$1/\chi \quad \alpha \ (T-T_c)$$

where, χ is the magnetic susceptibility, T_c is the Curie temperature and T is the applied temperature. Hence, it can be stated that a decrease in temperature below the Curie temperature will increase the net magnetic moment of the film. It can be seen from Figures 5.16 and 5.17 that the magnetic moment of all samples at 10K is much greater than that at 100K. The magnetic

moment per unit volume of LMO deposited on MgO is highest at 10K and 100K compared to the rest of the LMO films due to better epitaxial quality of this film. The lower than expected value of the magnetic moment for the LMO-LAO film might be the result of its partially defected or amorphous-like structure as shown by TEM.

Also, a temperature dependent magnetization study was performed in the range of 20-300K with constant applied field of 200 Oe, as shown in Figure 5.18. Bulk LMO is antiferromagnetic and its Neel temperature is 140K. Hence, under 140 K, the magnetic moments of molecules align in a regular pattern with neighboring spins (on different sublattices) pointing in opposite directions As the temperature is increased towards the Curie point, the alignment (magnetization) within each domain decreases. Above the Neel temperature, LMO behaves as a paramagnetic material. The results from Figure 5.18 show that the polycrystalline film LMO-S exhibits a phase transition at 140 K and that the epitaxial LMO films deposited on LAO and MGO show a phase transition at 150K and 160 K, respectively. This transition temperature is better than that previously reported by Aruta and coworkers[25]. They reported a transition temperature of 130 K for the LMO films deposited by the PLD process. The epitaxial film contains ordered arrays of neighboring spins of electrons hence, behaves as a single crystal. Therefore, the increase of magnetic transition temperature is seen to be increased than that of the polycrystalline film. Thus, the higher magnetic transition temperature observed in the present films attests to their high epitaxial quality.

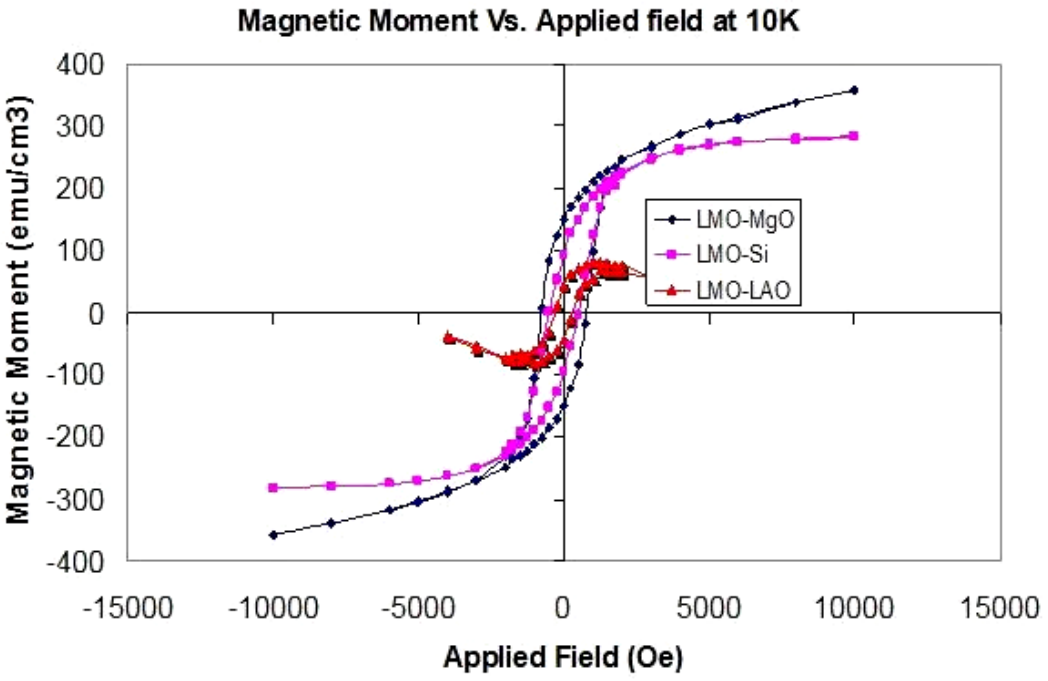

Figure 5.16 Hysteresis Loop for LMO thin films deposited on Si, MgO and LAO at 10K.

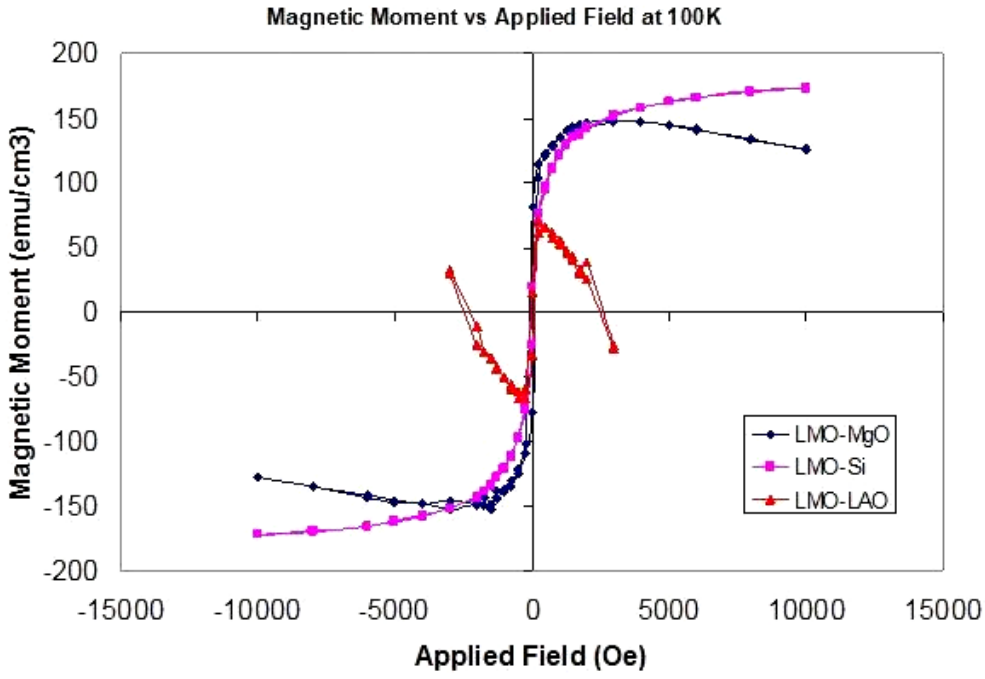

Figure 5.17 Hysteresis Loop for LMO thin films deposited on Si, MgO and LAO at 100K.

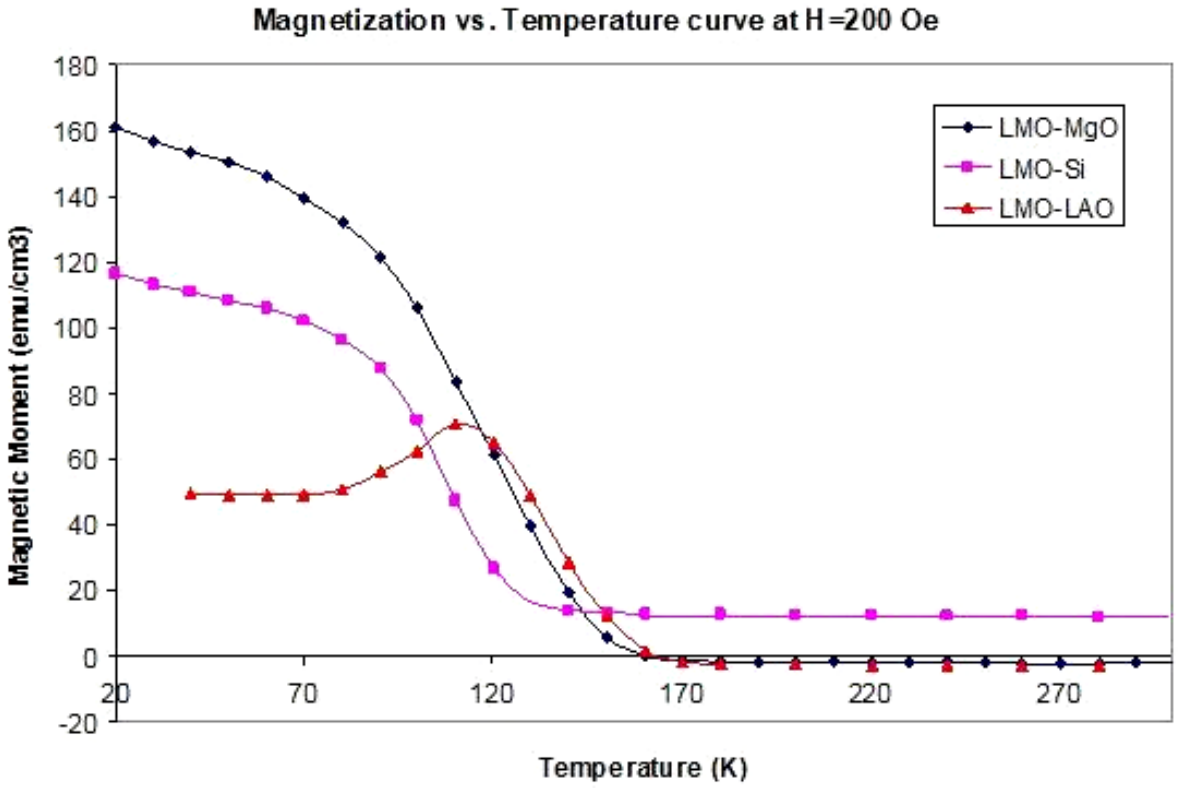

Figure 5.18 Temperature dependent magnetization for LMO thin films deposited on Si, MgO and LAO.

CHAPTER 6

CONCLUSIONS

1. Processing conditions were determined from a preliminary study to deposit good quality, undoped LMO films on Si by RF magnetron sputtering.
2. In process of synthesizing LMO-Si films, the effect of applied power and substrate temperature was investigated. The study revealed that the films exhibited amorphous-like structure if deposited at 700^{o}C substrate temperature and good quality polycrystalline structure for deposition at 750^{o}C temperature. The decrease in RF power leads to a better crystallinity in the film.
3. The processing conditions of good quality polycrystalline LMO-Si film were used for LMO thin film deposition on MGO and LAO substrates. Films deposited on these substrates exhibited a very good epitaxial quality.
4. Annealing experiment conducted on as-deposited LMO films showed that, heating at 800^{o}C in oxygen atmosphere filled the oxygen deficiency in as-deposited LMO films, promoting elemental stoichiometry and improved crystallinity.
5. AFM results showed that the surface of the epitaxial film was flat and homogeneous while the polycrystalline film exhibits a surface covered with submicron grains. The EFM images for on MGO and Si films show no change compared to the topography image.
6. The SQUID results showed that, the magnetic phase transition temperature found in polycrystalline films was 140K and that of epitaxial films was 160K; an increase in 10-30K than reported in previous studies.

REFERENCES

1. J.M.T. Thompson, *Visions of the future, physics and electronics*, 81.
2. J.C. Jiang, K. Gnanasekar and E.I. Meletis, "Composition and growth-temperature effect on the microstructure of epitaxial $La_{1-x}Sr_xMnO3$ (x = 0, 0.2) thin films on (001) $LaAlO_3$", *J. Mater. Res*., Vol. 18, 11, (2003), 2556-2561.
3. A. Barnabe, M. Gaudon, C. Bernard, C. Laberty, B. Durand, "Low temperature synthesis and structural characterization of over stoichiometric $LaMnO_3$ perovskites", *Materials Research Bulletin*, Vol. 39, (2004), 725-735.
4. R. Von Helmholt, J. Wecker, B. Holzapfel, L. Schultz, and K. Samwer, "Giant negative magnetoresistance in perovskite like LaBaMnO ferromagnetic films", *Phy. Rev. Lett.*, Vol. 71, 14, (1993), 2331-2333.
5. G.L. Bertrand, G. Caboche, L-C. Dufour, "Low-pressure-MOCVD $LaMnO_{3-\delta}$ very thin films on YSZ (100) optimized for studies of the triple phase boundary", *Solid State Ionics*, Vol. 129, (2000), 219–235.
6. O.Y. Gorbenko, O. Stadel, G. Wahl, A.R. Kaul, "MOCVD of LaMnO3 on biaxially textured Ni-based substrates in a reducing atmosphere", *Chemical Vapor Deposition*, Vol. 10, 2, (2004), 109-113.
7. Youichi Shimizu and Tomohiko Murata, "Sol–Gel synthesis of perovskite-type lanthanum manganite thin films and fine powders using metal acetylacetonate and poly (vinyl alcohol)", *J. Am. Ceram. Soc*., Vol. 80, 10, (1997), 2702–2704.
8. Tomohiko Nakajima, Tetsuo Tsuchiya, Masaki Ichihara, Hideaki Nagai, and Toshiya Kumagai, "Epitaxial growth mechanism for perovskite oxide thin films under pulsed laser irradiation in chemical solution deposition process", *Chem. Mater.*, 2008, Vol. 20, 7344–7351.

9. Q. X. Jia, T. M. Mccleskey, A. K. Burrell, Y. Lin, G. E. Collis, H.Wang, A.D. Q. Li and S. R. Foltyn, “Polymer-assisted deposition of metal-oxide films” *Nature Materials*, Vol. 3, (2004), 529-532.
10. V.M. Goldschmidt. Geochemische verteilungsgesetzte der elemente, VII, VIII, 1927-1928.
11. Y.Tokura,”Colossal magnetoresistive oxides”, Gordon and Breach Science publishers, 3.
12. J. H. Van Santen, G. H. Jonker, “Electrical conductivity of ferromagnetic compounds of Mn with perovskite structure”, *Physica*, Vol. 16, 7-8, (1950), 599-600.
13. C. Zener, “Interaction between the d-shells in the transition metals. II. ferromagnetic compounds of Mn with perovskite structure”, *Phys. Rev.*, Vol. 82, 3, (1951), 403-405.
14. H. Y. Hwang, T. T. M. Palstra, S-W. Cheong and B. Batlogg, “Pressure effects on the magnetoresistance in doped Mn perovskite”. *Phys. Rev. B*, Vol. 52, 21 (1995), 15046-15049.
15. Lei Wang, Xiaozhong Zhang, *Physica C*, Vol. 371, (2002), 330–338.
16. J. M. D. Coey and M. Viret, "Mixed-valency manganites", *Advances in Physics*, Vol. 48(2), (1999), 167-293.
17. K. Kubo and N. Ohata, “A quantum theory of double exchange”, *J. Phys. Soc. Jpn*., Vol. 33, 1, (1972), 21-32.
18. E. O. Wollan and W. C. Koehler, “Neutron diffraction study of the magnetic properties of the series of $La_{1-x}Ca_xMnO_3$ perovskite-type compounds”, *Phys. Rev.*, Vol. 100, 2, (1955), 545-563.
19. P. Shiffer, A. P. Ramirez, W. Bao, and S-W. Cheong, “Low temperature magnetoresistance and the magnetic phase diagram of $La_{1-x}Ca_xMnO_3$”, *Phys. Rev. Lett.*, Vol. 75, 18, (1995), 3336-3339.
20. A. Urushibara, Y Moritomo, T. Arima, A. Asamitsu, G. Kidoa, and Y. Tokura. “Insulator-metal transition and giant magnetoresistance in $La_{1-x}Sr_xMnO_3$”, *Phys. Rev. B*, Vol. 51, 20, (1995), 14103-14109.

21. J. B. Goodenough and A. L. Loeb, “Theory of ionic ordering, crystal distortion, and magnetic exchange due to covalent forces in spinals”, *Phys. Rev*., Vol. 98, 2, (1955), 391-408.

22. Julia M. Phillips, “Substrate selection for high-temperature superconducting thin films”, *J. Appl. Phys.*, Vol. 79, 4, (1996), 1829-1848.

23. S. Pignarda, K. Yu-Zhangb, Y. Leprince-Wangb, K. Hanc, H. Vincenta, J.P. Senateur, “Correlation between magnetoresistive properties and growth morphology of La_{1-x} $MnO_{3-\delta}$ thin films deposited on $SrTiO_3$, $LaAlO_3$ and MgO”, *Thin Solid Films*, Vol. 391, (2001), 21-27.

24. K.P. Ko, G.M. Shin, R.K. Ko, S.H. Moon, S.S. Oh and S.I. Yoo, “Processing and characterization of LaMnO3-buffered layer on IBAD-MgO template”, *Physica C*, Vol. 468, (2008), 1597–1600.

25. C. Aruta,a M. Angeloni, G. Balestrino, N. G. Boggio, P. G. Medaglia, and A. Tebano, “Preparation and characterization of LaMnO3 thin films grown by pulsed laser deposition”, *J. App. Phy.*, Vol. 100, (2006), 023910-023910/5.

26. A. Gupta, T. R. McGuire, P. R. Duncombe, M. Rupp, J. Z. Sun, W. J. Gallagher and Gang Xiao, “Growth and giant magnetoresistance properties of La-deficient $La_xMnO_{3-\delta}$ (0.67<x<1) films*”, Appl. Phys. Lett.*, Vol. 67, 23, (1995), 3494-3496.

27. G.J. Chen, Y.H. Chang, H.W. Hsu and Y.L. Chai, “Effect of substrate dependence on microstructure and magnetoresistance of lanthanum manganite films”, *Mat. Sci. and Engg. B*, Vol. 84, (2001), 182–188.

28. V.A. Shchukin, N.N. Ledenstov, P.S. Kopev, and D. Bimberg, “Spontaneous ordering of arrays of coherent strained islands”, *Phys. Rev. Lett.*, Vol. 75, (1995), 2968-2971.

29. Seung-Iel Park, Ji-Hee Son, Soung Suk Cho, and Chul Sung Kim, “Magnetoresistive and Magnetic Properties of RF-Magnetron Sputter Deposited La-Ca/Sr-Mn-O Films”, *IEEE TRANSACTIONS ON MAGNETICS*, Vol. 36, 5, (2000), 2933-2935.

30. “Synthesis structure and characterization of silver doped diamond like carbon thin films”, Pankaj Hazarika, MS Thesis.
31. K. Nakano, M. Naoe, M. Yamasaki, K. K. Choi, T. Taniyama, and Y. Yamazaki, "Bias dependent intergrain tunneling in lanthanum manganite thin films", *IEEE TRANSACTIONS ON MAGNETICS*, Vol. 35,5, (1999), 2859-2861.
32. W. Tang, T. Kam and J. Gao, “Deposition of high quality CMR thin films by rf magnetron sputtering under pure argon gas*”, Materials Research Bulletin,* Vol. 36, 7-8, (2001), 1463-1469.
33. L. Malavasi, M. Mazzati, I. Alessandari, L. Depero, C. Azzoni, G. Flor, “Thin films of sodium-doped lanthanum manganites: role of substrate and thickness on the magnetoresistive response”, *Solid State Ionics*, Vol. 172, (2004), 265–269.
34. K. T. Jacob and M. Attaluri, “Refinement of thermodynamic data for $LaMnO_3$”, *J. Mater. Chem.*, Vol. 13, (2003), 934–942.
35. J. D. Suh, G. Y. Sunga, K. Y. Kanga, H. S. Kimb, J. Y. Leeb, D. K. Kimb and C. H. Kimb, "Cubic Y–Ba–Cu–O thin films by high speed pulsed laser deposition", Physica C Superconductivity, Vol. 308, 3-4, (1998), 251-256.
36. "Quantum chemistry of solids: The LCAO first principles treatment of crystals", Springer Publications, Edition 1, (2007), 386.
37. C. Cibert, M. Chatras, C. Champeaux, D. Cros and A. Catherinot, “Pulsed laser deposition of aluminum nitride thin films for FBAR applications”, *Applied Surface Science*, Vol. 253, (2007), 8151–8154.
38. Kiyotaka Wasa, Yoko Haneda, Toshifumi Satoh, Hideaki Adachi and Kentaro Setsune, “Sputtering deposition of perovskite thin films with atomic-scale controlled surface”, *Applied Surface Science*, Vol. 121 -122, (1997), 152-155.
39. Xin Chen, NaiJuan Wu, John Strozier and Alex Ignatiev, “Spatially extended nature of resistive switching in perovskite oxide thin films”, *App. Phy. Lett.* Vol. 89, (2006), 063507.

BIOGRAPHICAL INFORMATION

Varad Rajan Sakhalkar was born on January 8, 1985 in Ratnagiri, India. He attended the Shirke School, during which time he earned awards in National School Scholarship Exam and National Talent Search examinations. He appeared 27th in the state merit list and graduated in 2000.

During his undergraduate program at the Government College of Engineering, Pune (COEP), he researched on “Synthesis, characterization and analysis of polymer/clay nanocomposites” at the National Chemical Laboratories, Pune, and received his Bachelor of Engineering in Metallurgical Engineering in 2006. He then studied at the University of Texas at Arlington, where he researched on “Structural, magnetic and surface properties of RF magnetron sputter undoped lanthanum manganite thin films” and received his Master of Science in Materials Science and Engineering in December of 2009.

Immediately after graduation, Varad was offered a permanent position as Ceramic Development Engineer at Rubicon Technology in Chicago, IL, which he accepted and is currently working there.

His hobbies are badminton, chess, digital photography and astronomy.